Evaluation of Mechanical Properties of existing reinforced concrete bridges

Alberto Sánchez Palomera

2022

Structural Engineering, Bachelor's level

Luleå University of Technology

Department of Civil, Environmental and Natural Resources Engineering

Division of Structural and Fire Engineering

LULEÅ UNIVERSITY OF TECHNOLOGY

Acknowledgements

I would like to express my deepest gratitude to my thesis supervisor, Gabriel Sas (Professor and Head of Subject), for the giving the opportunity to work in such a great and supportive working team. Furthermore, I could not have carried out this work without my thesis co-supervisors, Jaime Gonzalez-Libreros (Postdoctoral Researcher) and Silvia Sarmiento (PhD Student); I am more than grateful for their feedback and patience throughout the whole research.

I am also thankful to all the LTU Department of Civil, Environmental, and Natural Resources Engineering. And especially, my lab mates, Erik Andersson, Vanessa Saback, Mats Petersson and Mert Pinar, for their guidance and care during the experimental work. Thank you also to the Universidad de Zaragoza (Unizar), for giving me the opportunity to expand my horizons and discover a whole new world in the North of Sweden through the Erasmus+ scholarship.

Lastly, I would like to thank my parents, my sister and my closest friends. Their belief in me has been unconditional and has helped me during these months, making me maintain motivation.

Abstract

The mechanical properties assessment of existing structures is important to analyse the behaviour of the structure, and to predict the possible behaviour of other similar structures, or structures under similar load cycles, which is the focus of this paper.

Analytical and numerical methods have been carried out over samples extracted from a real structure (a 65-year-old bridge in Kalix, northern Sweden), over cast cylinders, and over samples extracted from a full-scale trough bridge model cast at Luleå University of Technology (LTU). The methods or tests used at the LTU laboratory are three-point bending test, tensile test, and compressive test. These tests were performed following previous studies and considerations from different researchers. Moreover, Finite Element Models (FEM) were developed to compare the results of both analytical and numerical methods.

Results from the mentioned tests and Finite Element Models are presented and summarized in this paper. The analytical methods have shown that the mechanical properties of the old Kalix bridge are better than expected, since it was a 65-year-old structure, and the obtained values for Fracture Energy and the rest of mechanical properties are really similar to the ones obtained through testing overcast cylinders and extracted cylinders from the trough bridge.

Keywords: Fracture energy, concrete, mechanical properties, tests, core samples, beams, notch.

Table of contents

1. Introduction

1.1. Background

Concrete is a heterogeneous material. This means that when analyzing the mechanical properties of a given structure, they can vary depending on the place where samples are taken. It is basically made up of cement paste and rock particles. More specifically, concrete, seen from a mechanical point of view, is a two-phase material, which means its properties vary depending on the state it is in. In the first of the states, concrete is a two-phase material composed of a *"continuous matrix"* of cement paste and fine aggregates and is known as "the mortar phase". The second of the states is the "aggregate phase", in which the concrete is a *"particulate dispersion"* of coarser aggregates than in the earlier one. The definition of these two distinct phases is especially important when analyzing the influence of both the aggregate and the mortar-aggregate interface on concrete fracture.

In order to determine the behavior of existing concrete bridges, it is important to carry out tests to obtain the mechanical properties of the material. Those mechanical properties may change throughout the time, depending on the climate factors such as cold temperatures, the loading cycles provoked by vehicles or snow, among other things.

The aim of this research study is to compare different methodologies to determine the mechanical properties of concrete, especially the Fracture Energy. In fact, the Fracture Energy is the focus of this thesis, since plays a significant role when analyzing the numerical assessments of concrete structures. Different numerical and analytical methods have been carried out throughout the years in order to calculate the Fracture Energy of concrete. Unfortunately, it is not possible, as of today, to perform accurate enough in-situ tests over existing structures. Then, the only way to carry out tests for existing structures is to take out samples and test them at a laboratory. Therefore, this is the procedure followed during this paper.

In this thesis, the results of tests performed to obtain the concrete mechanical properties for two different case studies are presented. The first case study corresponds to a 65-year-old prestressed concrete bridge located in Kalix, northern Sweden, and the second corresponds to two reinforced concrete trough bridges cast in laboratory at the beginning of 2022.

The results were obtained from performing compression and tensile tests on cylindrical specimens extracted from the Kalix bridge and cast trough bridges. In addition, diverse types of specimens from the trough bridge concrete in the form of rectangular beams, cylinders and cubes were cast in the laboratory of the Luleå University of Technology and tested. Furthermore, the results were used to calibrate the finite element models of the samples.

1.2. Aim and Objectives

When numerically evaluating existing structures, it has been found that the magnitude of the concrete fracture energy has a significant influence on the accuracy of the predicted behavior. The aim of this thesis is to validate a newly developed experimental methodology based on a uniaxial tensile test to assess the fracture energy of existing concrete structures, which will reduce the uncertainties related to this mechanical property.

The objectives of this thesis are:

- To carry out an extensive literature review of the available experimental methods to evaluate the fracture energy of concrete.
- To obtain concrete samples extracted from two types of structures.
- To perform tests to evaluate the most important mechanical properties of concrete.
- To perform and compare two different experimental methodologies for the concrete fracture energy assessment.
- To develop Finite Element Models of the samples tested.

1.3. Research questions

This thesis aims to answer the following research questions:

RQ1: does the proposed methodology for the evaluation of concrete fracture energy provide adequate results?

RQ2: what are the parameters that influence the results of the fracture energy obtained through the proposed methodology?

2. Literature review

2.1. General

According to various sources, Fracture Energy (usually represented as G_F) can be described in diverse ways, but all these ways share certain aspects. First, Fracture Energy can be understood as the amount of energy that is necessary to produce a crack in a unit of area (Peterson, P. E. (1980)). It can also be said that "the area under the common tensile softening curve or the curve of cohesive stress and crack opening of a fictitious crack determines the specific fracture energy G_F" (Duan, K., Hu, X., & Wittmann, F. H. (2007)). Facture Energy can be described, as well, as the criterion used to figure out the energy consumption needed for crack propagation in any material and, in our case, in concrete. According to Hillerborg, A. (1985), the area enclosed under the load-deflection curve obtained from a specimen corresponds to the total energy absorbed in a stress test performed up to fracture. The total energy absorbed can be divided into two parts. The area enclosed under the stress-strain curve represents the energy per unit volume, which is absorbed by the whole specimen. On the other hand, the area enclosed under the cohesive stress-crack opening curve stands for the energy absorbed in the damage zone. The latter area stands for the Fracture Energy per unit area in the fracture surface. Finally, some define the so-called "cohesive energy fracture", which is "is the external energy supply required to create and fully break a unit surface area of the cohesive crack and is given by the area under the softening function" (Elices, M., Rocco, C., & Roselló, C. (2009)).

2.2. Methods for quantifying Fracture Energy

Nowadays, there is a diverse number of methods for quantifying Fracture Energy. This might lead to large variations in the obtained Fracture Energy values, depending on the method or approach used. The variability on the methods are the result of the different modifications and improvements among them, which came with the necessity of reach more accurate values.

2.2.1. Three-Point Bending Test (3PBT)

3PBT is a widespread method for calculating and assessing the mechanical properties of different types of materials, whether they are fibers (Mannocci, F., Sherriff, M., & Watson, T. F. (2001)), metals such as aluminum (Zu, G. Y. et al. (2013)) or aluminum and steel alloys (Omerspahic, E. et al. (2006)) and, of course, to concrete, which is the main focus of this paper. In order to perform the 3PBT, different recommendations have been added over the years to obtain more reliable results, for instance the recommended estimated error, geometry of the specimens, among others. This way, the protocols that have been followed over the years are explained in this section.

In his studies on the rate of energy released (G_C), which was later used to determine the Fracture Energy (G_F), Peterson, P.E. (1980) pointed out that the results obtained using the 3PBT with a notch can be useful if Linear Elastic Fracture Mechanic (LEFM) is implemented, as long as the maximum applied load is known.

However, the results provided by this method are not the most proper when it comes to calculating the energy needed to cause a fracture in materials such as concrete or its derivatives, so the concept of Fracture Energy was proposed. The amount of energy needed to produce a crack per unit area, as well as the principle for measuring G_F, hold when both the crack propagation and the energy consumed in such propagation are on the right path.

In order for the fracture energy results obtained using the 3PBT method to be sufficiently adequate or appropriate, the amount of energy contributed by the beam's weight and by applying an external load must be equal to the amount of energy consumed in the crack propagation process.

When evaluating the test results from the 3PBT method, it should be considered that the fracture energy values are the effect of the applied load and the weight of the beam. In some cases, the effect of the beam weight in terms of energy can be eliminated by considering that the total length of the beam is twice the distance between the supports. Shorter beam lengths can also be used, but in this case, the moment produced by the beam weight must be compensated by using additional weights at the beam ends. However, the use of beams in this method may have certain inconvenients. In order to avoid these drawbacks, the only possibility is to consider the weight of the tested beam.

The International Union of Laboratories and Experts in Construction Materials, Systems and Structures (RILEM), but more specifically Hillerborg, A (1985), made a series of recommendations to improve the tests proposed by Peterson years ago. To analyze the tensile stiffness of concrete, the most systematic, rapid, and proper method is fracture mechanics. To perform this test, certain prerequisites are necessary. First, the specimen to be tested must be manageable and easy to handle, so that the risk of damaging or destroying the specimen is minimized. Second, the depth and width of the fracture area should not be less than one third of the total aggregate size. Thirdly, the energy absorption that occurs in the zones that do not belong to the fracture area should be minimal. Finally, the stiffness demand on the machine on which the test is conducted must be limited, i.e., it is necessary that the method is stable and reliable, and the tests performed following the procedure can be carried out in other laboratories, no matter the quality of the laboratory.

Guinea, G. V., Planas, J., & Elices, M. (1992) proposed a model highlighting the most decisive aspects when estimating the error that occurs when quantifying the Fracture Energy, which are various. In addition, they stated that the residual force influences the tail of the graph that cannot be neglected in those methods in which the intermediate moments are eliminated.

The European standard (En, B. S. (2007)) approach sets up some geometrical and compositional parameters for the samples. Moreover, it states that there has to be a rigid frame in the middle of the span of the supports, and at mid height of the beam that is to be tested. A displacement transducer (LVDT) is allocated on the frame.

In addition to the methods mentioned above, there are additional 3PBT methods that are considered less conventional for measuring fracture energy. Among them, we can highlight the method proposed by Malvar, L. J., & Warren, G. E. (1988). In this method, instead of being placed under the test beam, it is placed on the top surface. The beam is supported by 4 springs which, in turn, are aligned with the rollers. These rollers are placed on bearing pads to minimize the energy dissipated at the bearing points. On the other hand, another non-conventional method is the realization of a 3PBT method in a semicircle. The latter method is mainly used in the

cohesive crack model (which is discussed later in Section 2.2.3) to investigate and analyze fracture parameters in road constructions.

2.2.2. Four-Point Bending Test (4PBT)

To carry out this method, the configuration to be performed is very similar to that of the three-point bending test, with the difference that, in this case, the force applied on the upper surface is divided into 2 points, and distributed equally on both sides of the notch, instead of applying all the load on the notch in the center of the beam. In the same way, the number of Linear Variable Displacement Transducers (LVDTs) increases by the same amount. This test is carried out following the indications provided by the Italian UNI Code for fiber reinforced concrete (FRC). The 4PBT provides results on first crack strength, nominal stresses, maximum bending stresses, material ductility indices, and material ductility index and about crack mouth opening displacement (CMOD) and crack-tip opening displacement (CTOD). In addition, a positive point about this method is that the fracture energy can be obtained directly from the load-displacement curve, the fracture energy being the area below the CMOD curve. In the 4PBT method, the area between the two points where the loads are applied is under pure bending, so shear does not contribute to the failure of the beam. On the other hand, the bending moment required for crack propagation to occur when the beam is subjected to pure bending is greater than the shear moment.

2.2.3. Cohesive crack model

The original "fictitious crack model" was renamed to "cohesive crack model". It is used for brittle or quasi-brittle materials, as it is accepted as a realistic simplification of the fracture of these types of materials. In this model, the whole fracture process is aligned, which allows the specimen to be treated as elastic. For this purpose, it has to be assumed that "a cohesive crack initiates at the point where the maximum principal stress σ_l first reaches a critical value called the cohesive strength σ_t" (Elices, M. et al. (2009)). This cohesive crack is formed in the either in the normal or the orthogonal direction of the major principal stress, forming a 90 degrees angle. Moreover, since this stress is induced by the notch, when the cohesive crack starts forming, follows the path initiated by the notch. After crack formation, the crack opens, transmitting the stress from one side of the crack to the other. Once the crack has been initiated, following the direction marked by the notch, the transferred stress (also called cohesive stress) is a function dependent on the creation of the crack.

2.2.4. The compact tension test (CTT)

In order to evaluate the Fracture Energy of concrete, Wittmann, F. H. et al. (1988) proposed a new method, the Compact Tension Test. Prior to this study, the use of this method was restricted to examining the fracture path and evaluating the fracture behavior of materials other than concrete, such as metals, asphaltic concrete (Wagnoner, M. P. et al. (2005)) or ceramics and nanoceramic resin composites (Badawy, R. et al. (2016)). Nowadays, the CTT is mainly used to evaluate the parameters and characteristics of concrete or asphalt pavements, or various binder

materials. The fracture parameters of the material tested are assessed using this so-called Modified Compact Stress Test (MCTT). For that purpose, cylindrical-shaped specimens are used. The high versatility this method offers is its major advantage, since it can be applied both to laboratory samples and to specimens extracted directly from existing structures. In order to carry out this method, the center of the specimen analyzed is the maximum depth that the crack reaches. In addition, with the purpose of evaluating the fracture parameters, reinforcing steel bars are used. After completion of the relevant tests on the specimens, the fracture energy results obtained using the MCTT are compared with a finite element simulation.

2.2.5. The wedge splitting test (WST)

Brühwiler, E., & Wittmann, F. H. (1990) proposed this new method for calculating Fracture Energy over cubic or cylindrical concrete samples, based on the results proposed by Linsbauer, H. N., & Tschegg, E. K. (1986). This new method overcomes the disadvantages of the likes of 3PBT and CTT methods. It is used to quantify the fracture parameters of concrete and concrete-like materials. In order to carry out with this testing method, both a wedge and a notch are created. They can be created by mechanizing it (using a saw) or, when the concrete samples are cast, using a mold with the specified shape. This method minimizes the effect of beam weight on fracture energy measurement, which, compared to the 3PBT and CTT methods, is a great advantage. Normally, when performing this procedure, cubic specimens are used from freshly cast concrete, while cylindrical samples are taken from existing structures. In addition to the advantage mentioned above, this method is especially useful in checking the condition of the specimens, and the likelihood of specimens breaking during testing or handling is minimal.

2.2.6. Uniaxial tensile test (UTT)

The direct tension method was initially used over cylindrical samples without a notch (Rusch, H., & Hilsdorf, H. (1963); Hughes, B. P., & Chapman, G. P. (1966); Evans, R. H., & Marathe, M. S. (1968)). Nevertheless, as time went by, the method incorporated the use of a notch at the middle of the specimen. In addition, the geometrical parameters of specimen size and shape, as well as the manner in which loads are applied to the specimens, have changed dramatically. With all these changes applied to the original procedure, the new improved method is known as Uniaxial Tension Test. Nilimaa, J., & Nilforoush, R. (2020) performed this method at Luleå University of Technology over cylindrical samples extracted from a real bridge located in Kiruna, northern Sweden, as well as over core samples cast in the laboratory. To proceed with this method, it is necessary to first ensure that the applied loads are always maintained in the same line of action, in order to prevent the occurrence of eccentric loads and to maintain the clamping conditions correctly. For that purpose, the core samples' ends need to be prepared prior to the test, by polishing the surfaces and cleaning them. These samples' ends are glued to loading plates, where the load is applied.

2.2.7. Kazemi, M. T. et al. (2007) model

Kazemi et al. (2007) performed 3PBT over a standard cylindrical in order to evaluate the Fracture Energy. In the proposed method, the use of fibers has no effect on the maximum applicable force, and its major influence is on the amount of fracture energy in the post-peak zone of the concrete. Furthermore, except for a small amount of energy dissipation in the vicinity of the notch, the rest of the energy required is contributed by crack propagation.

2.2.8. Duan, K. et al. (2013) bilinear model

Duan, K. et al. (2003) stated that the first report about the size effect on the fracture properties for concrete materials was from Kaplan, M. F. (1961, November). Moreover, Duan, K. et al. (2003) developed the concept of localized Fracture energy proposed by Hu, X. Z., & Wittmann, F. H. (1992 & 2000) by introducing a bilinear model for the boundary or size effect in binders. The goal of this method was to develop a new way for determining fracture energy that is doesn't depend at all on the specimen size. In order to create this method, it was assumed that the crack is created along the desired crack path. This model is based on the proportional relationship between the localized fracture energy and the fracture process zone (FPZ) height. In other words, Duan, K. et al. (2003) developed a bilinear model in order to assess the size effect on the fracture properties of concrete structures, that links directly the Fracture Process Zone (FPZ) and the Fracture Energy of the sample. By using the bilinear model, it is possible to find the reduction in the fracture process zone height as it approaches the specimen boundary.

2.2.9. Size-independent method

It has been stated by many authors that the shape and size of the specimen affects directly to the results of specific Fracture Energy, since the free surface of the specimen influences the local energy in the fracture process. Vydra, V. et al. (2012) proposed a new concept of local Fracture Energy, applying 3PBT, bit the crack is modeled as an "elastically equivalent notch", where the effective crack length is equal to the depth. This method presents the advantage of using less samples of different shapes, notch to depth ratios or sizes. Then, the calculation of the size independent Fracture Energy is greatly simplified.

Teng, S. et al. (2014) examined models on the effect of size and presented a new method comparing such size-independent models. They found that the use of the size effect in Bažant's theory, although it reduces the size effect on fracture energy, has 2 drawbacks. First, the size of the largest specimen should be at least 4 times larger than the size of the smallest specimen. The second is that only the maximum force is considered and therefore the post-peak displacement has no effect. The method they proposed, based on nonlinear regression, has the best predictive ability of the displacement at failure compared to the rest of the proposed methods.

2.2.10. Meso-mechanical model

Snozzi, L. et al. (2012) presented an innovative computational model with the purpose of investigating the mechanical response of concrete specimens or samples tested to dynamic compressive and tensile loading. This new model combines the interface debonding and the frictional contact, and it consists in modelling concrete using a meso-mechanical approach. By applying it, all the material parameters can be physically assessed. The Fracture Energy is measured throughout the application of this method as the confining pressure is augmented. Snozzi, L. et al. (2012) concluded that the rise in strength is directly linked to a higher Fracture Energy dissipation.

Huang, J., & Li, V. C. (1989) derived analytic expressions for Fracture Energy and for the tension softening curve. They based their studies in previous studies from Hillerborg, A. (1985). Nevertheless, they concluded their study stating that the interchange between Fracture Energy and tensile strength only describes the normal strength concrete behavior, and not for high strength concrete.

2.3. Comparison between different methods

The size-independent method is used to investigate the effect of structural elements on the capacity limit state used in the design. The initial fracture energy (G_f) is calculated using beams with the same geometrical characteristics but varying their sizes at maximum load and at the slope prior to the peak of the load-displacement curve. On the other hand, for the determination of the fracture energy (G_F), beams are simply used to check the behavior and characteristics of the concrete, through the determination of the fracture energy of the total work exerted on the concrete softening curve. The size effect plot has 2 strength criteria as well as several LEFM regions. The larger the specimen, the closer the failure is located to the point of maximum load. Therefore, LEFM can be used on long beams in the size effect method to determine both the effective structural dimension and the brittleness number.

The determination of the relationship between G_F and G_f is of vital importance. Problems in fracture energy (G_F) variations in different dimensions, problems related to energy consumption by specimen weight, the drawback of fictitious energy at the tail of the load-displacement curve and crack deflection out of the fracture process zone leading to higher energy consumption can be reduced or even eliminated.

2.4. Factors that affect Fracture Energy results

Since some experiments or methods are conducted to obtain the Fracture Energy values, the results will depend not only on the method used, but also on other distinct factors. For example, if the composition of two concretes is different, obviously the mechanical properties of these concretes will be different as well. Another example is the existent relation between water and cement in the composition, whose ratio (water to cement) will also vary the mechanical properties of the different composites. These are the first two factors to be listed. However, there are a wide variety of factors, which will be explained below.

2.4.1. The aggregate composition

The aggregate is the most critical part within concrete. The structure of the concrete holds itself thanks to the aggregate. If concrete without aggregate is evaluated, the results will show that the mechanical properties of it are not the best ones. Some investigations have shown that, among the concrete, the cement paste and the mortar, it is the concrete which has the highest Fracture Energy associated. The higher the coarse aggregate is, the longer the crack path the crack has to open in the tested specimen. In addition, the aggregate produces what is known as "interlocking". As Ioannides, A. M., & Korovesis, G. T. (1990) stated, the aggregate interlock is a “natural mechanism effective in transferring loads across discontinuities, such as joints and cracks, in […] cement concrete pavement systems”. Interlocking occurs between different aggregates and, therefore, the energy needed for crack propagation increases considerably.

2.4.2. The water to cement ratio

As Khalilpour, S. et al. (2019) stated, the water to cement ratio can directly affect the Interfacial Transition Zone (ITZ). Then , it is safe to say that it plays an especially vital role in determining the Fracture Energy of concrete. In Wittmann, F. H. et al. (1987) studies, different mechanical parameters of the cement, such as fracture energy, elastic modulus, and tensile strength, are shown in the graphs, depending on the water to cement ratio. Fracture energy is calculated in two diverse ways. First, using the load-deflection diagram (method explained below). Second, using an empirically obtained equation. Either way, the value of all mechanical parameters, including Fracture Energy, decreases as the water to cement ratio increases. This is because the higher the water content in the mix, the higher the porosity, which leads to the existence of a greater number of microcracks. If this happens, the microcracks would eventually coalesce, resulting in a much larger crack, which would result in less energy absorbed and, therefore, a reduction in the Fracture Energy.

2.4.3. The specimen size & the notch to depth ratio

Studies from Mindess, S. (1984), Wittmann, F. H. et al. (1990) and Bazant, Z. P., & Planas, J. (2019) show that the tensile strength is lower, and the brittleness of the material is higher as the size of the specimen tested is increased. As the size is increased, the path that the crack creates when the fracture process is initiated is longer. Thus, the Fracture Energy is increased. Mihashi, H. et al. (1991) applied the Wedge Splitting Method in their studies, and they got to the conclusion that the Fracture Energy values obtained through this method were higher as the dimensions of the specimen were higher as well. Therefore, it is safe to state that for smaller specimens the effect of the size is smaller. Nevertheless, Jueshi, Q., & Hui, L. (1997) determined Fracture Energy results by applying 3PBT. They calculated the Fracture Energy of beams that were short (the largest one was 400mm), and the results obtained by them reported that the Fracture Energy was decreased as the size was increased. Moreover, they realized that the size effects were decreased when the size in mortar specimens was increased. In addition, the consumed energy of the crack propagation decreases if the notch to depth ratio is increased.

2.4.4. The use of natural fibers

The use of fibers in concrete, both natural and artificial, has become widespread in recent years, as they improve in a non-negligible way the mechanical performance of concrete and, therefore, increase its energy absorption capacity. When improving the mechanical properties of concrete by using fibers, different actions can be carried out, such as varying the type of fiber, modifying the fiber density, using fibers with different ultimate tensile strengths, etc. The durability and properties of concrete are improved when using fibers: flexural strength, toughness, impact stress, fatigue resistance, vulnerability to cracking and spalling. When introducing fibers into the concrete, they can be of diverse types, giving rise to what is known as a "hybrid mix". When using this new hybrid mix of fibers, it is important to consider the type, the size and the number of fibers used, as well as their overall contribution. In addition, with the use of fibers, the ductility of the concrete can range from just a few millimeters to several centimeters. Basically, the job that fibers do when they are applied to concrete is to achieve greater control over the cracks that may appear, as well as to give it greater fracture toughness. (Explain the interaction between different kind of fibers and its results).

As Barros, J. A., & Sena-Cruz, J. (2001) stated in their study, steel fibers are the most widely used for concrete reinforcement in the construction industry. The reasons why their use is so widespread are their economy, manufacture facilities, reinforcing effects and resistance to the environment aggressiveness. Their studies came to several conclusions. Among them, the higher the fiber density, the higher the maximum stress. In addition, the energy absorption capacity increased almost linearly with fiber content. However, it is difficult to achieve a homogeneous fiber distribution.

2.4.5. The change of concrete mixture

Monteiro, P. J., Helene, P. R., & Kang, S. H. (1993) conducted experiments in which they changed the concrete mixture in order to test how the strength, elastic modulus and Fracture Energy varied. For this, they used a mix designed nomogram, keeping the water to cement ratio constant, which was based on several previous studies. Six different mix proportions were used, and compressive strength, splitting tensile strength, elastic modulus, Fracture Energy and characteristic length were figured out. The parameters modified in the concrete mixture were the water to cement ratio (modifying both water and cement), the fine + coarse aggregate to cement ratio, the entrapped air, the slump and specific weight. Therefore, by having so many variables, the results of the mechanical properties are truly diverse, depending on the modified parameters. For example, the Fracture Energy values that were obtained when the cement content is decreased or the aggregate content is increased are different, depending on the water to cement ratio (if $^{W}/_{C}$ ratio is constant, G_F is higher), or the workability (if the workability is constant, lower G_F values are obtained).

2.4.6. The curing temperature

The reason concrete is so widely used globally as a reliable all-weather material is its high tolerance and versatility when working with it in different temperatures. However, it should be noted that there are environments in which temperatures oscillate between the positive and

negative parts of the Celsius scale, leading to so-called freeze-thaw cycles. Constantly rising and falling below zero degrees Celsius increases the porosity of the concrete, as water freezes and thaws accordingly. Therefore, the performance of the concrete may be affected, and internal and external cracks may appear. If these freeze-thaw cycles occur more often, the fracture energy will be higher, as the water will affect the micro-cracks in the concrete. Bažant, Z. P., and Prat, P. C. conducted experiments in which the temperature was varied to see if, consequently, the Fracture Energy varied in the same way. The conclusions they reached with the results obtained were the following. Firstly, the law of size effect can be applied to a wide range of temperatures, ranging from room temperature up to even 200ºC. Its parameters depend on two factors: the temperature and the water content of the concrete. It was further concluded that the Fracture Energy is directly dependent on the curing temperature. Thus, as the temperature increases, the Fracture Energy slowly decreases. On the other hand, the effect of the water content of the specimens was practically null at room temperature and had a great relevance at higher temperatures (around 100ºC).

2.4.7. The age of loading

Keeping the water to cement ratio constant, Wittmann, F. H., Roelfstra, P. E., Mihashi, H., Huang, Y. Y., Zhang, X. H., & Nomura, N (1987) tested specimens to measure the mechanical parameters of Fracture Energy, elastic modulus and tensile strength as a function of the time the cement had cured. In these experiments, it was shown that the 3 mechanical properties increase as the curing time increases, but, after a certain time (approximately 2 weeks), the curves of the properties become linear. In particular, the Fracture Energy and tensile strength stabilize around a certain point, while the elastic modulus increases slowly. This is because the concrete solidifies as time passes until, at a certain point, there is no more mixture in a liquid state that can solidify.

Wittmann, F. H. (1992) conducted again the experiment of modifying the age of loading, obtaining very similar results to those obtained years ago. The Fracture Energy increases as the elapsed time increases, for the same reason explained above.

In the following Section 3, the parameters that were modified to carry out the tests are detailed.

3. Methodology

3.1. General aspects

Previously, some of the methods that can be used to quantify Fracture Energy have been briefly explained in Section 2. However, not all described methods were conducted in this study; therefore, in this section the tests and methodologies carried out in laboratory are explained.

In order to assess the possible differences between the Fracture Energy values obtained through different methodologies, some tests were carried out in laboratory. First, a case study of two trough concrete bridges is used to compare different methodologies. The trough bridges were cast in laboratory at LTU and samples were collected from the different concrete batches (beams, cylinders and a slab, see Figure 1).

Figure 1: Concrete samples and slab cast in laboratory at LTU; divided in batches

For this first case study, 3PBT was performed over the cast beams, and the results are compared to the ones obtained through the proposed methodology based on uniaxial tensile tests, which were carried out over the cast cylinders and extracted cores from the slab.

Then, a second case of an existing prestressed concrete bridge was studied, which corresponds to the old Kalix bridge. Since it is an existing structure, only samples of concrete cores were possible to be extracted from the structure. These samples were used to perform uniaxial tensile and compressive tests.

The obtained experimental results for both case studies are compared to the ones obtained using Finite Element Modeling, which were calibrated and can be later used for sensitivity analysis.

The different considerations for the tests, as well as the geometrical parameters of the specimens are discussed in this section, together with the machinery necessary to carry out the tests. Analytical formulations and desired results are also described.

3.2. Tests to determine Fracture Energy

3.2.1. 3PBT

As explained in the Literature Review, different considerations can be used when proceeding with the Three-Point Bending Test (Figure 2). First, the weight of the beam will be considered to be zero in order to calculate the fracture energy. To do so, one can proceed in two separate ways. In the first case, the total length of the beam should be equal to twice the distance between the supports (Figure 3). In the second, shorter beams are used but, in this case, the moment produced by the weight of the beam must be compensated by using weights at the ends of the beam (Figure 4). The equation to calculate the Fracture Energy with both methods is the following:

$$G_F = \frac{A_1}{b(d-a)} \qquad (3.2.1.1)$$

where b, d and a are geometric parameters (being beam width, beam depth and notch depth, respectively) and A_1 is the whole area enclosed under the load-deflection curve.

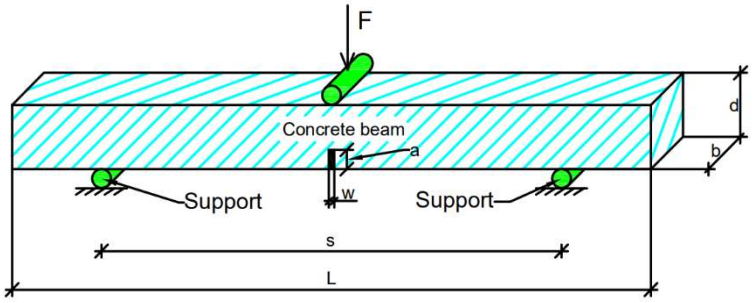

Figure 2: Three-point bending test. "a" and "w" are the notch depth and width respectively, "d", "b" and "L" are the beam depth, width and length respectively, and "s" is the span between the supports.

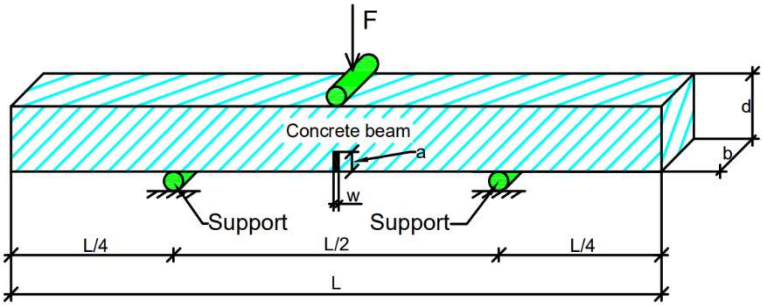

Figure 3: Three-point bending test, not taking in consideration the beam weight since the length of the beam is twice the length between the supports.

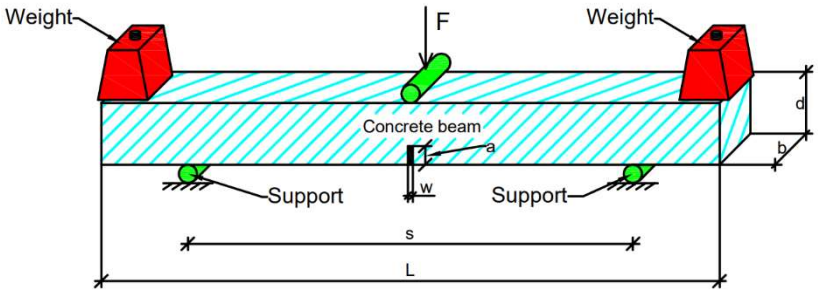

Figure 4: Three-point bending test, compensating the beam weight with two additional weights in the ends of the beam.

However, the use of these two methods may incur certain problems. Among these drawbacks, we can point out that the use of beams that are too long can lead to problems in performance tests. In addition, when performing the load-deflection curve (Figure 5), a long tail (which may approach infinity) will be produced. The problem this causes is that, when quantifying the area enclosed under the curve, a planimeter will be used. On the other hand, it is important that the system is balanced because, if it is not, the long tail can cause problems. Ideally, we would like to be able to stop the tests at a certain time, of our choice, so that the above-mentioned errors do not occur. Notwithstanding, this is only possible if the weight of the tested beam is considered.

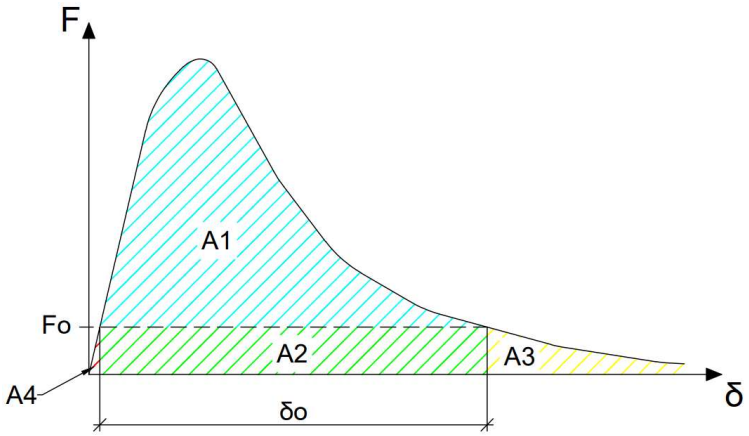

Figure 5: Load-Deflection variation curve, where F is the load applied and δ is the deflection

If the beam is unbalanced due to the beam effect, then the beam will fail at the F_0 point of the load-deflection curve. To calculate F_0, the following equation will be used:

$$\frac{F_0 l}{4} = \frac{mgl^2}{8} => F_0 = \frac{mgl}{2} = \frac{Mg}{2} \qquad (3.2.1.2)$$

where m is the mass per unit length in the beam, M is the full mass of the beam and g is the acceleration of gravity with value $g = 9'81\,{}^{m}/_{s^2}$.

Once F_0 is obtained, we can calculate the Fracture Energy:

$$G_F = \frac{A_1 + A_2 + A_3 + A_4}{b(d-a)} \quad (3.2.1.3)$$

where A_1 (blue), A_2 (green), A_3 (yellow) and A_4 (red) are the areas shown in Figure 4.

A_1 can be calculated using a planimeter and, according to Petersson, P. E. (1981), the following equations are used to calculate A_2 and A_3:

$$A_2 = A_3 = \frac{Mg\delta_0}{2} \quad (3.2.1.4)$$

Since A_4 is insignificant compared to the rest of the areas, it can be neglected. Then, the equation for calculating the Fracture Energy is the following:

$$G_F = \frac{A_1 + Mg\delta_0}{b(d-a)} \quad (3.2.1.5)$$

where δ_0 is the deflection at the end of the fracture process.

There is still a remaining amount of inelastic energy in the stress-strain curve, in the tension zone, which lies outside the fracture zone. Therefore, better results or at least more proper results would be obtained by making use of complex Finite Element Mechanics (FEM) methods. Still, the mentioned method is good enough if the aim is to obtain acceptable Fracture Energy results.

The recommendations that Hillerborg, A (1985) proposed in his studies on the calculation of Fracture Energy can be applied to the previous method. The requirements mentioned in the Literature review on how to proceed with the tests should not be forgotten, although it is impossible to fulfill all of them since some of them are contradictory. However, certain compromises can be reached. In addition to these recommendations, the term "work of fracture" was also proposed, with the ultimate aim of calculating the Fracture Energy more accurately.

As Kozłowski, M. et al. (2015) stated, Fracture Energy can be either obtained through Equation 3.2.1.5, by first obtaining A_1 as the area under the load – displacement curve, or as the area under the Load – CMOD curve.

The following equations will allow us to calculate the work of fracture:

$$W = W_0 + W_1 + W_2$$

with,

$$W_1 = F_0 \cdot \delta_0$$

Furthermore, Petersson, P. E. (1981) stated and proved that W_1 (green; Figure 6) and W_2 (yellow; Figure 6) are equal and, as it has been explained previously, W_0 is obtained using a planimeter. Then, the work of fracture will be:

$$W = W_0 + 2F_0 \cdot \delta_0 \qquad (3.2.1.6)$$

With the above expressions, the Fracture Energy can be defined as follows:

$$G_F = \frac{W + (m_1 + 2m_2)g\delta_0}{b(d-a)} \qquad (3.2.1.7)$$

Where m_1 is the mass of the beam multiplied by the length of the beam, and m_2 is the loading set-up.

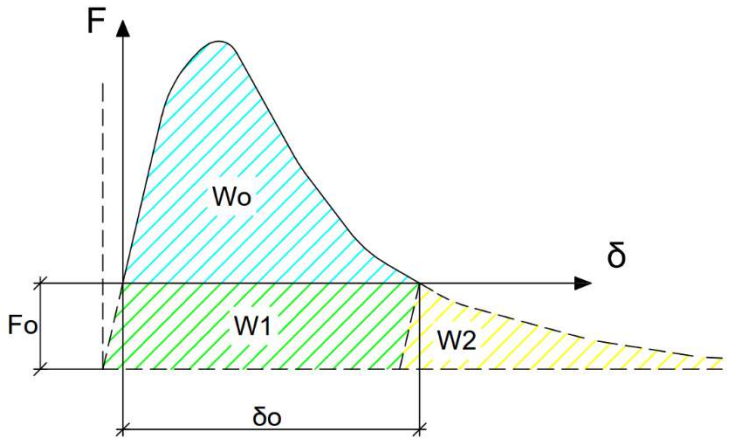

Figure 6: Load - Deflection curve

In the laboratory, the three-point bending test were conducted on the cast beams, and the equation recommended by Hillerborg in 1985 (3.2.1.5) were used to calculate the Fracture Energy value.

3.2.2. Uniaxial tests

Uniaxial tests were carried out in cores obtained from the Kalix bridge, as well as in cores obtained from a slab and cylinders cast directly in the lab from the trough bridges concrete. These kinds of tests are carried out to obtain some of the concrete mechanical properties of both case studies. Data from the geometry of the samples was collected after the samples' preparation.

3.2.2.1. Compression tests

Compression tests are methods used for assessing the mechanical properties of a vast variety of materials. In order to measure the compressive strength, there are different compression test methods. Three different compression tests are explained, but only one was carried out at LTU lab. As Nordlund et al. (2006) stated, in the uniaxial compressive test, the specimens are loaded with a slowly increasing axial stress, as shown in Figure 7. Once the failure load is obtained, the uniaxial compressive strength can be calculated. Other different method mentioned by Nordlund et al. (2006) is the point load test, and it can be used as well for the obtention of the

compressive strength. In this case, the load is applied in just two points. If it is applied to a cylinder, these two points can be at the bottom and at the top of the sample, or the load can be applied at two points of the lateral surface. The last method mentioned by Nordlund et al. (2006) is the Triaxial compressive test. In this test, the load is applied in all the sample. If the sample is cylindrical, the load is applied in both top and bottom faces, as well as in the lateral surface. Out of these three methods, the one carried out in the lab is the first one, the uniaxial compressive test.

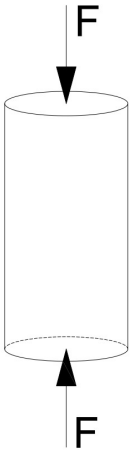

Figure 7: The principle for uniaxial compressive testing. The load is applied to the whole top and bottom end's surface

3.2.2.2. Tensile tests

The tensile tests were carried out in the specimens. It is a widely known method used for determining mechanical properties of the specimens, like the existent relationship between tensile stress and tensile strain, as well as the ductility of the material (Komori, K. (2019), or the Modulus of Elasticity. It can be applied to many varied materials such as concrete or steel. There are two separate ways of carrying out this method: the direct tensile test (such as tensile test) and the indirect tensile test (such as Brazilian test). As Zheng et al. (2001) assessed, the tensile strength value obtained through these two methods is different. The direct tension test methods offer results closer to the real value of tensile strength when the specimens are under an axial load that applies pure tension. Therefore, in this case study, the applied method is the direct tensile test. In Figure 8, the schematic drawing of the tensile test is shown.

The method proposed in this study to obtain the fracture energy used is a variation of this tensile test, based on Nilimaa, J., Nilforoush, R., Bagge, N., & Elfgren, L. (2020) work. The modification done is that a notch is created at the half of each core (i.e., the notch is at the same distance from the top and the bottom of the cylinder), using a lathe. This way, the cross-section area of the core sample at the notch is smaller than the original one. The layout of this tensile test variation is shown in Figure 9.

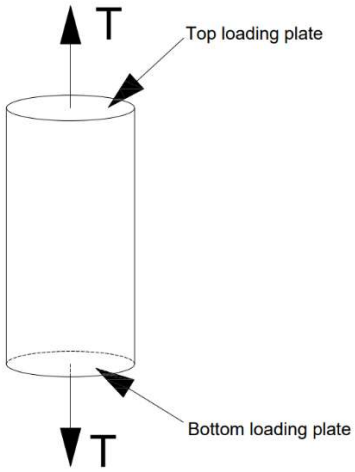

Figure 8: The principle for uniaxial tensile testing. The load is applied to the whole top and bottom end's surface, by using loading plates

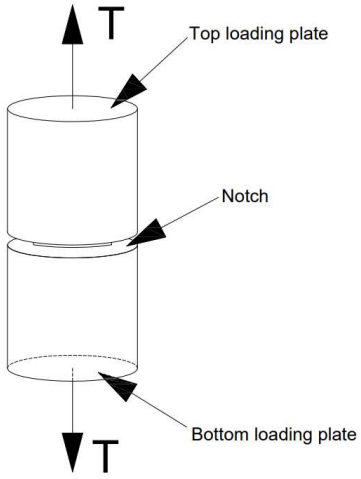

Figure 9: The principle for uniaxial tensile testing, with the proposed variation.

3.3. Finite Element Models (FEM)

In addition to performing the tests in the laboratory, finite element models were also developed using ATENA Science V.5.9. software. With this program, it was modeled the 3PBT of the notched beam, the tensile stress test of the notched cores, and the compression tests of the cores without a notch. In this way, the results obtained from the FEM analysis can be compared with those obtained experimentally. The results provided by the program can be compared and calibrated with the experimental values. The details of the models and results are explained in Section 5.2.

4. Experimental work

The content of this section is based on an explanation of the work performed in the concrete laboratory at Luleå University of Technology, as well as the field work carried out at Kalix Bridge. Therefore, both the tests set-up and execution are discussed, together with the additional activities performed that contributed to the development of this thesis.

4.1. Trough bridge case study

4.1.1. General aspects

At Luleå University of Technology, two full-scale trough bridges were cast, which are going to be tested in the future. A trough bridge consists of two longitudinal concrete beams that supports a concrete slab, as shown in Figure 10, and together help to contain the ballast, the sleepers and the rails.

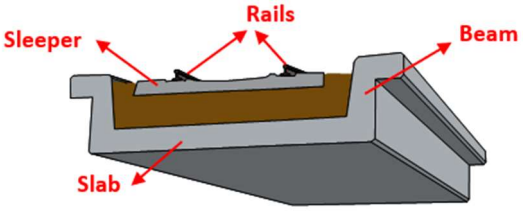

Figure 10: Main layout of a concrete trough bridge

The geometry of both cast bridges are included in Appendix 1. Basically, they are roughly 6.1m long, 4m wide and 1.02m high but, as it can be seen in Appendix 1, it is more complex than that. In the following Figure 11 and Figure 12, the cast process of both trough bridges is shown:

Figure 11: Casting Day; Trough bridge #1 being cast

Figure 12: Casting Day; View from the two cast trough bridges

During the casting day it was collected samples from the concrete batches. A total of 18 cubes, 30 cylinders, 12 beams and a concrete slab were cast, some of the samples are shown in Figure 13 and Figure 14. For obtaining the cores from the slab, the diamond coring tool for wet drilling Hilti DD 200-CA Core Drill was used again, just like it was used at Kalix' bridge.

Figure 13: Cast cubes and cylinders in laboratory at LTU

Figure 14: Cast beams in laboratory at LTU

Different experiments were carried out to obtain Tensile Strength, Compressive Strength and the Fracture Energy values. G_F results were obtained by using the data collected from uniaxial tensile tests, uniaxial compressive tests and three-point bending tests.

Among all these methods performed, the 3PBT is carried out with the purpose of obtaining only the Fracture Energy values. The uniaxial tensile test can be used for obtaining values of both Tensile Strength and Fracture Energy. Compressive tests are used to obtain values of Compressive Strength, which can be used to calculate the Young Modulus and Fracture Energy using analytical formulations.

4.1.2. Instrumentation and casting of the full-scale trough bridges

Although the activities described in this section are not directly related to the aim and objectives of this thesis, they contributed to the knowledge and experience in laboratory work.

As mentioned previously, two full-scale bridges were cast at LTU in order to test their capacity and study their behavior. Prior to the cast, the bridges were instrumented by installing fiber optic sensors (FOS) and strain gages to the reinforcement steel bars (see Figure 15, Figure 16, Figure 17, Figure 18, Figure 19). Both the FOS and the strain gages were glued to the reinforcement bars, so that the strains while performing the tests can be assessed and measured precisely.

Figure 15: Reinforcement bars for cast trough bridges

Figure 16: Bar polishing process in order to glue a strain gage

Figure 17: Strain gage glued to a reinforcement bar

Figure 18: Installation process of the FOS on reinforcement steel bars

Figure 19: FOS installed and glued to a reinforcement steel bar

4.1.3. Tests

Tensile test

The tensile strength, σ_t, is obtained through the testing over core samples. For that purpose, the ends of the cylinders were cut with a saw (see Figure 21), and then polished using a lathe (see Figure 20), so that the surface is smooth. The surfaces must be parallel to each other, so that the load is applied correctly and thus the results are valid. After the polishing of the surfaces, a notch of 3mm width is created in the middle of the cylinder using the lathe again, and the depth of this notch is desired to be 15mm in radius or, in other words, 30mm. For calibrating

the lathe in order to create the notch, a dial gauge and a 70mm diameter form are used (see Figure 22).

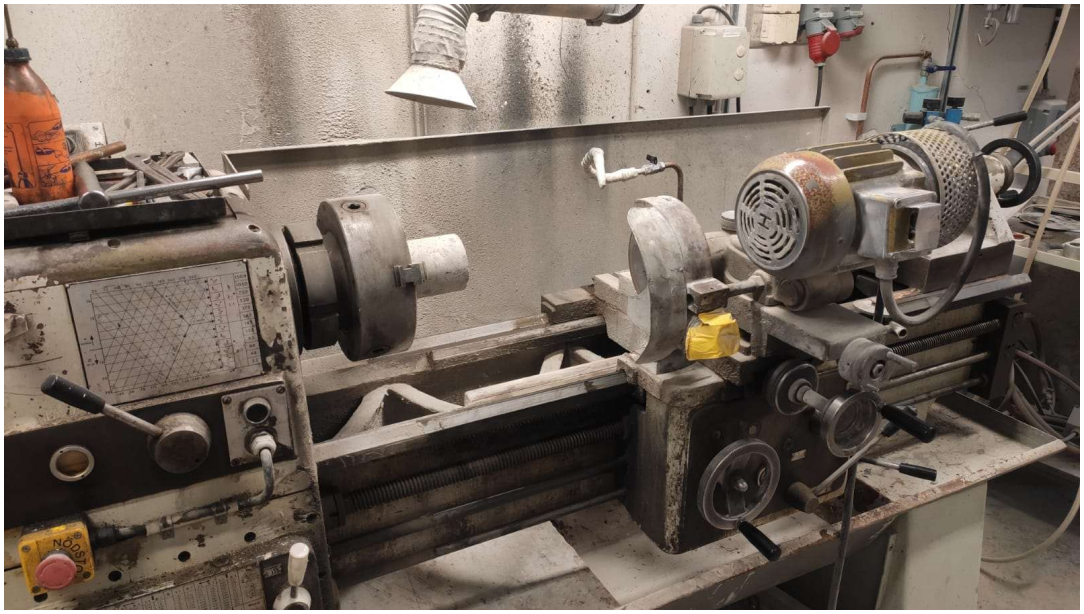

Figure 20: Lathe used for polishing the core samples surfaces, as well as for notching

Figure 21: Saw used for cutting the ends of the core samples

Figure 22: Dial gauge (right) and the 70mm diameter form (left) used for calibrating

Nevertheless, the core samples needed to be re-notched. Therefore, it needs to be considered that each turn of the dial gauge equals 1mm, and the final notch depth was up to 20mm in radius.

After this mechanization performed over the samples, they needed to be prepared for the test. Therefore, the ends of the cylinders were polished again, as well as the plates (see Figure 24) where the cylinders were allocated subsequently, but this time, a sandpaper with a 180 number grit was used. Right after the polish process, all the surfaces needed to be clean. First, a layer of

acetone was applied. Since acetone provokes problems when gluing, the acetone needed to be cleaned, using isopropanol.

Once all the surfaces are smooth and clean, they were glued using a two-phase glue (X60-NP, see Figure 23). This two-phase glue consists of a powder (Component A) and a liquid (Component B). The hardening time of the glue is, at least, of half an hour. The gluing process is as it follows: First, the bottom of the core sample is glued to one of the plates, and some pressure is applied to the top surface. When the glue is hard enough, the other part of the cylinder is glued to the plate, but this time the hydraulic press is used. A load of 0.2kN is applied while the glue hardens.

Figure 23: Two-phase X60-NP glue. Powder component (left) and liquid component (right)

Figure 24: Loading plate, where the core sample is glued using X60-NP

Right after that, the test is ready to be started. The displacement rate was 0.05 µm/s at the beginning. However, once the load reached 0.5kN, this displacement rate was increased to the double, i.e., to 0.1 µm/s, so that the testing was faster. Everything is monitored in real time, so that if there is some failure, it can be assessed fast.

Figure 25: Direct tensile test being performed and monitored in real time

The tensile strength of the core samples can be obtained using the following equation:

$$\sigma_t = \frac{T_{Max}}{A}$$

Where T_{Max} is the failure load and A is the cross-section area of the core sample at the notch.

In the following Figure 26 and Figure 27, the outline of a core sample is shown. COD stands for "Crack-Opening-Displacement." In other words, the CODs are the instruments (gauges) used for measuring the crack width once the test is being performed. It needs to be mentioned that this is an example, and that not all the samples will be 150mm long, and not all of them had a diameter of 60mm at the notch section.

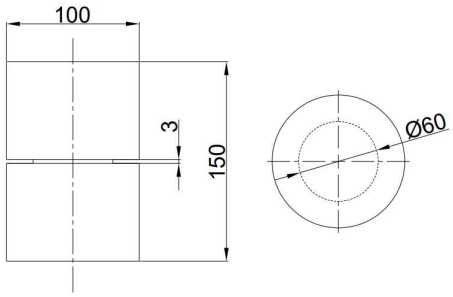

Figure 26: Geometry of the core sample

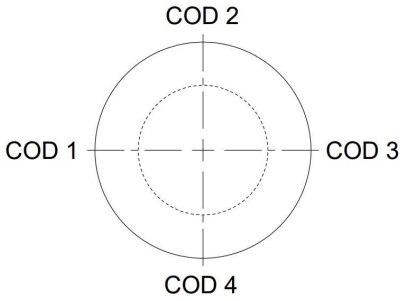

Figure 27: COD layout

The following Figure 28 and Figure 29 show the main layout for a core sample in order to carry out the tensile test. The CODs (gages) are the green instruments. As it can be seen, the plates are attached to the hydraulic press using six bolts.

Figure 28: Tensile test layout for a concrete core (1)

Figure 29: Tensile test layout for a concrete core (2)

Compressive test

Compression strength is one of the main parameters that need to be considered when the mechanical properties of a material like concrete are assessed. The foundations of the bridge need to bear huge loads due to the weight of the bridge, as well as the variable loads provoked by the weight of the vehicles, people, snow, or many other factors. passing by the bridge. Therefore, the compressive strength of cores from the bridge will be assessed, as well as the cast cores and the cores from the slab.

In order to measure the compressive strength, compression tests are carried out over the samples. For that purpose, the specimens were prepared prior to these tests, the same way as they were prepared for the tensile test. More specifically, the core samples were prepared using a saw (see Figure 21), to remove the superficial imperfections, or the parts that could interfere in the results of the experiment. After cutting the ends of each core, they were polished using a lathe (see Figure 20). The surfaces of the top and bottom of the cylinder need to be smooth and parallel to each other, so that the testing is performed correctly, and the results are valid.

Then, a hydraulic press is used to perform the test (see Figure 30). Once the test is done, the maximum load is obtained as the fracture load. With the maximum load the sample can bear and the cross-section area of the cylinder (at any point, the diameter is the same for all the length), the compression strength, σ_c, is calculated using the following equation:

$$\sigma_c = \frac{F_{Max}}{A}$$

Where F_{Max} is the maximum load and A is the cross-section area of the core sample.

Figure 30: Hydraulic press used for Compressive tests

Modulus of Elasticity

The Young's Modulus, or Modulus of Elasticity, can be easily obtained through the tensile tests. For that purpose, the Stress – Strain curve has to be plotted. The elastic part of the curve is the first one, i.e., where the curve is a straight line. Therefore, the Elastic Modulus can be obtained through:

$$E = \frac{Stress\ (MPa)}{Deformation} = \frac{\sigma_x}{\Delta L}$$

Where x is any point belonging to the straight line. This means that E is the slope of this straight-line. Then, it is easy to obtain it plotting the curve and calculating the straight-line equation $y = mx + n$. m is the desired Young's Modulus' value.

Nevertheless, it cannot be calculated through the tensile test that has been performed at the concrete lab, because the core samples used had a notch at the middle of it. Therefore, the cross-section area at the notch is smaller than the cross-section area at any other part of the core sample. Moreover, the tests that were carried out had the specifical parameters for obtaining results for Fracture Energy. Then, the tests were not appropriate for calculating the Modulus of Elasticity.

A separate way for obtaining the modulus of elasticity is using the uniaxial compressive strength. For any kind of concrete (high strength concrete, HSC ,or normal strength concrete, NSC), the Comité Euro-International du Béton and the ENV 1992-1-1 (Eurocode 2) propose a relation between the compressive strength of the concrete and the Elastic Modulus, as it follows:

$$E = 22000\left(\frac{\sigma_c}{10}\right)^{1/3}$$

Where σ_c (in MPa) is the uniaxial compressive strength of the concrete, obtained through compressive tests. The result of Elasticity Modulus is obtained is in MPa.

A second approach can be used for HSC. It was proposed by ACI Committee 363. (1984), and it is a function of both the uniaxial compressive strength and the density of the concrete studied:

$$E = (3321{\sigma_c}^{0.5} + 6895) \cdot \left(\frac{\rho}{2300}\right)^{1.5}$$

Where σ_c (in MPa) is the uniaxial compressive strength of the concrete, obtained through compressive tests, and ρ is the density of the concrete, in kg/m^3.

The third and last approach is proposed by the Architectural Institute of Japan (1985):

$$E = 21000\left(\frac{\rho}{2300}\right)^{1.5} \cdot \left(\frac{\sigma_c}{20}\right)^{0.5}$$

Where σ_c (in MPa) is the uniaxial compressive strength of the concrete, obtained through compressive tests, and ρ is the density of the concrete, in kg/m^3.

However, as Noguchi, T. et al. (2009) stated, the effectiveness of these proposed equations is debatable. These relationships may work for NSC, but not for HSC, because in the HSC the

Elasticity Modulus depends greatly on the coarse aggregate. Thus, it is suggested to measure the Young Modulus directly for HSC, and not through the empirical approaches mentioned before.

Fracture Energy

In order to obtain Fracture Energy, two different types of tests were carried out. The first one was the 3PBT, which it was performed over the cast beams. Then, uniaxial tensile tests were performed over the core samples obtained from the Kalix bridge, the cast cylinders and the core samples taken out from the slab. The reason for using two different tests to obtain the Fracture Energy value is to compare and check that the proposed methods are correct and well performed.

Beams of different lengths were available, and they were cast with concrete of different batches (there were four different batches in total). There were two different kinds of beams cast, depending on their length. Some of them were 600mm long, and the rest were 1000mm long. The widths and depths of all of them were 75mm and 125mm, respectively, for all of them.

For the purpose of this Thesis, only the beams from the first batch (Ba_1) will be tested to 3PBT.

Once the beam measurements were taken, a notch was created in the middle of each beam, as required by the 3PBT. The depth of this notch (a) is approximately equal to 0.33 times the width of the beam. In other words, since the results obtained for width were between 125mm and 130mm, the depth of the notch should be between 41.67mm and 43.33mm.

After notching the beams, they were prepared for the DIC (Digital Image Correlation) system. For this purpose, one of their faces (from now on, the front face) was painted white, using a spray paint, and two layers were applied. Then, small black dots were painted on the same front face. In this way, with the *ARAMIS* software, the damage and deformation caused by the applied load can be evaluated. However, the analysis of the DIC data is out of the scope of this thesis. The displacement rate was 0.1µm/s.

Figure 31: 3PBT main layout for a cast concrete beam

The main layout consists in 2 supports, which are steel cylinders. They are placed at the same distance from the notch. Depending on the length of the cast beam, the distance from the support to the end, at each side, is larger or smaller. In the upper part, there is a loading plate together with another cylinder. It is, through this cylinder, that the load is applied to the beam. This last cylinder has to be aligned with the notch, so that the test is carried out correctly.

At the bottom part of the beam, the two-phase glue X60-NP is used for attaching two small edges to each side of the notch (see Figure 23). First, the edges' surfaces and the beam's surface where the edges were desired to be glued were polished, using a 180 sandpaper. Then, the edges were glued, with a separation of 10mm; the notch was at the middle of them. Then, a COD gauge is used and placed between the edges (see Figure 32), in order to measure the Crack-Opening Displacement. With all these considerations and preparations, the 3PBT was ready to be performed.

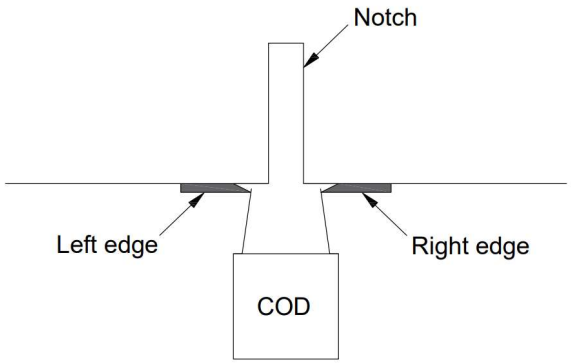

Figure 32: Outline of the glued edges and the COD gage for the cast beam

The proposed compressive test and tensile test methods mentioned previously not only serve to calculate the compressive strength and the tensile strength respectively, but also, they can be used to assess the Fracture Energy of all the concrete samples as well. Therefore, many results obtained through different tests were evaluated and analyzed. This way, these results are compared to each other, and a conclusion can be stated.

4.2. Kalix bridge case study

4.2.1. General aspects

At Kalix, concrete cores were extracted from the 65 years old bridge to analyze them back at LTU (see Figure 34). The bridge has a total length of 283'6m and a width of 13m and consists of 5 spans. It is a symmetrical bridge around the midpoint of the midspan, and the length of the spans are 43'85m (outer spans), 47m (inner spans) and 94m (console span), as shown in the following Figure 33. The outer spans correspond to the sections 1-2 and 5-6; the inner spans correspond to the sections 2-3 and 4-5; the console/2 span corresponds to the section 3-4.

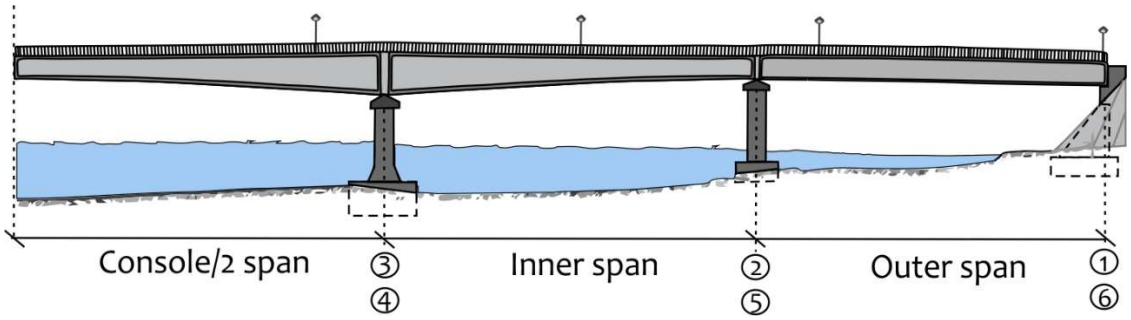

Figure 33: Main layout of the 65 years old Kalix bridge spans. Only half of the bridge is represented since it is symmetrical

Figure 34: The 65 years old bridge situated in Kalix (Northern view)

4.2.2. In-situ work

Diamond coring tool

The extracted cores are cylinders of 100mm diameter (approximately) and of variable length. The length depended on the thickness of the zone where the cores were extracted. There could be steel tendons as well, that work as reinforcements for the bridge, so they needed to be avoided in order to obtain pure concrete core samples. For their extraction, a diamond coring tool for wet drilling was used (Hilti DD 200-CA Core Drill, see Figure 37), as shown in Figure 38.

In order to identify the position of the bars and tendons of the bridge, a cover meter (see Figure 35) was used, so that the extracted cores were just of pure concrete. Figure 36 shows where the tendons and bars were at one of the walls.

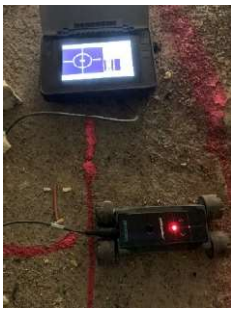

Figure 35: Cover meter for identifying the bars and tendons

Figure 36: Layout of bars and tendons of one of the Kalix' bridge walls

The installation process of the tool is as it follows: First, a hole of 12mm diameter is drilled in the wall or the floor, depending on where the core samples were going to be extracted. Then, a concrete-expander bolt is introduced in the hole, with the help of a hammer. Right after that, the tripod is placed in the desired position, and fixed to the wall/floor, screwing a nut onto the concrete-expander. The tripod has three bolts, whose function is to maintain the perpendicularity between the diamond coring tool and the surface where the core samples are taken out. A constant water flow is needed during the coring process, since it prevents overheating problems, and it works as a coolant.

The diamond coring tool has different operational modes. The core samples that were taking out had a diameter of approximately 100mm. Thus, the operational mode of Ø82-162 had to be selected. Moreover, the coring tool had to be hammering and drilling.

The cores were extracted from the bridge roof, as well as from the walls and floor of the bridge from each of the spans, as shown in Figure 38. With them, it is intended to measure the mechanical properties of the bridge's concrete, and we will analyze if there is any difference depending on the extraction zone.

Figure 37: Diamond coring tool for wet drilling Hilti DD 200-CA Core Drill

Figure 38: Core sample extraction process with the diamond coring tool for wet drilling (Hilti DD 200-CA Core Drill) at the Kalix bridge

In total, 120 core samples were extracted from the Kalix bridge, with the purpose of testing them so that the compressive strength, the tensile strength and the modulus of elasticity could be calculated. The cores were extracted from specifical positions along the bridge, in order to capture the spatial variability of the concrete in the existing structure. Nevertheless, not all of the results obtained from testing the cores are included in this paper.

Schmidt-hammer

The Uniaxial Compressive Strength (σ_c), of the Kalix bridge concrete can be assessed using a Schmidt-hammer (also known as rebound hammer). For that purpose, the rebound value is measured in all the spans of the bridge, in order to check if there was some kind of variation in the measurements. The measurements are taken in the same places where the cores are extracted from the wall. In the following Table 1, these measurements are listed for just one of the sections of the outer span (O3).

Figure 39: Schmidt-hammer test being carried out at one of the Kalix' bridge walls

Table 1: Rebound values measured at the Kalix bridge, for the outer span at the O3 section

Point	Rebound value			Mean value
1	50	46	51	48.95
2	45	47	45	45.66
3	41	40	42	40.99
4	39	38	31	35.82
5	43	42	43	42.66
6	43	44	42	42.99
7	44	45	42	43.65
8	43	48	46	45.62
9	46	48	45	46.32

The total mean value of all the results is obtained through the arithmetic mean:

$$Total\ mean\ value = \frac{\sum_{i=1}^{n} Mean\ value_i}{n} \quad (4.2.2.1)$$

Where n is the number of points assessed. Therefore, the total mean value is obtained: 43.48.

Once all the rebound values measurements are obtained, the chart for assessing the approximate uniaxial compressive strength σ_c is used, following the indications offered by ASTM, C. (2002) and ACI Committee 228--Nondestructive Testing of Concrete. (2003).

4.2.3. Tests

The carried-out tests for the concrete cores extracted from the Kalix bridge are the tensile test and the compression test. With both of them, the tensile strength, the compressive strength, the modulus of elasticity and the Fracture Energy are calculated. The way of proceeding with them is the same as mentioned previously for the trough bridge specimen testing, in Section 4.1.3.

5. Results & discussion

In this section, the results of the carried-out tests are presented and analyzed. Specifically, the aim of the section is to evaluate the Fracture Energy of the specimens, obtained through both three-point bending tests and tensile tests.

5.1. Analytical determination of mechanical properties

5.1.1. Compression test results

Compression tests were carried out in some of the samples in order to obtain the compression strength. In the following Table 2, the geometrical parameters of the core samples that were prepared specifically to perform the compression tests are listed.

The load rate applied through the hydraulic press to the core samples is set to 6.28 kN/s, except for the cores with an (*), whose load rate was 10kN/s. Moreover, a pre-load of 12 to 14kN is applied at the beginning of the test.

From each bridge span, core samples were taken out from 4 points from the inside of the bridge: the top slab, both walls and the bottom slab. The length of the core samples is desired to be either 100mm or 200mm. About the nomenclature of the core samples, for example the core O3-3-100 is take out from the point 3 of the outer span, and its length is about 100mm. In the following Table 2, Table 3, and Table 4, the geometrical parameters of the collected samples are listed.

Table 2: Geometrical parameters of core samples obtained from Kalix bridge outer span

Core tag	Core origin	L (mm)	Ø (mm)	A (mm^2)	W (g)
O1-2-100	Kalix bridge Outer span	100.45	99.30	7744.01	1.870
O1-5-100	Kalix bridge Outer span	102.43	99.29	7743.63	1.620
O2-3-100	Kalix bridge Outer span	96.81	99.26	7738.14	1.760
O2-5-200	Kalix bridge Outer span	210.25	99.31	7745.97	3.700
O3-3-100	Kalix bridge Outer span	106.25	99.40	7759.62	1.947
O3-3-200	Kalix bridge Outer span	197.50	99.36	7754.16	3.628
O3-4-100	Kalix bridge Outer span	105.75	96.65	7336.18	1.857
O3-5-200	Kalix bridge Outer span	204.75	93.96	6933.49	3.435

O3-6-100*	Kalix bridge Outer span	105.32	94.17	6964.89	1.7395
O4-3-100*	Kalix bridge Outer span	105.37	93.88	6922.81	1.720

L is the length of the core sample, Ø is the diameter of the core sample, A is the cross-section area of the core sample, at any point, W is the weight of the core sample.

Table 3: Geometrical parameters of core samples obtained from Kalix bridge inner span

Core tag	Core origin	L (mm)	Ø (mm)	A (mm^2)	W (g)
I2-5-100	Kalix bridge Inner span	104.82	94.64	7034.23	1.780
I2-6-200	Kalix bridge Inner span	213.37	94.52	7017.51	3.630
I2-10-100	Kalix bridge Inner span	107.95	98.34	7596.16	1.950
IW2-6-100	Kalix bridge Inner span	111.69	98.58	7632.12	2.015
IW2-6-200	Kalix bridge Inner span	193.50	98.56	7629.02	3.520
I3-2-100*	Kalix bridge Inner span	107.25	94.66	7038.29	1.789
I3-3-100*	Kalix bridge Inner span	95.52	94.87	7068.46	1.612

L is the length of the core sample, Ø is the diameter of the core sample, A is the cross-section area of the core sample, at any point, W is the weight of the core sample.

Table 4: Geometrical parameters of core samples obtained from the cast slab

Core tag	Core origin	L (mm)	Ø (mm)	A (mm^2)	W (g)
Slab_TB-1	Slab	161.75	97.0	7389.81	2893.0
Slab_TB-2	Slab	164.0	97.75	7504.53	2939.5
Slab_TB-3	Slab	164.5	97.75	7504.53	2877.5

L is the length of the core sample, Ø is the diameter of the core sample, A is the cross-section area of the core sample, at any point, W is the weight of the core sample.

The compressive strength, σ_c, is obtained by dividing the maximum load the core sample can bear (i.e., the fracturing load) by the cross-section area of the core sample. This compressive strength can be used for obtaining the Fracture Energy (G_F) of the concrete. Specifically, as Nilimaa, J., Nilforoush, R. et al. (2020) stated, in the CEB-FIP Model Code 1990 (2013), the following equation for assessing G_F was given:

$$G_F = \alpha_f \left(\frac{\sigma_c}{\sigma_{c0}}\right)^{0.7}$$

Where σ_c is the compressive strength of the analyzed concrete, $\sigma_{c0} = 10MPa$, and α_f is a coefficient that depends on the maximum grain size. The Fracture Energy, G_F, is obtained using the empirical formula given by the fib Model Code 2010 (2013), which is a modification of the previous one:

$$G_F = 73 \cdot {\sigma_c}^{0.18}$$

It needs to be mentioned that, for the longer cores (the ones whose length is more or less 200mm), a correction factor of 0.87 needs to be applied in order to obtain proper results for uniaxial compressive strength.

Therefore, in the following Table 5, Table 6, and Table 7, the results obtained from the compression tests are listed, together with the calculation of G_F for each core sample.

Table 5: Summary of the results obtained from compression tests over Kalix' outer span cores

Core tag	Core origin	F_{Max} (kN)	σ_c (MPa)	G_F (Nm/mm^2)	E (GPa)
O1-2-100	Kalix bridge Outer span	618	69.4291	156.603	41.970
O1-5-100	Kalix bridge Outer span	633	71.1178	157.282	42.307
O2-3-100	Kalix bridge Outer span	525	59.0258	152.093	39.759
O2-5-200	Kalix bridge Outer span	413	53.318	149.335	38.434
O3-3-100	Kalix bridge Outer span	526	58.9745	152.070	39.748
O3-3-200	Kalix bridge Outer span	459	59.194	152.171	39.797
O3-4-100	Kalix bridge Outer span	489	57.9907	151.610	39.525
O3-5-200	Kalix bridge Outer span	400	57.691	151.468	39.457
O3-6-100*	Kalix bridge Outer span	438.76	54.8065	150.076	38.788
O4-3-100*	Kalix bridge Outer span	416.62	52.3573	148.847	38.202

F_{Max} is the maximum load the core sample bears, σ_c is the uniaxial compressive strength of the concrete, G_F is the Fracture Energy, calculated using the fib Model Code 2010 (2013), E is the Elastic Modulus of the concrete, calculated using the expression proposed by the Comité Euro-International du Béton and the ENV 1992-1-1 (Eurocode 2).

Table 6: Summary of the results obtained from compression tests over Kalix' inner span cores

Core tag	Core origin	F_{Max} (kN)	σ_c (MPa)	G_F (Nm/mm^2)	E (GPa)
I2-5-100	Kalix bridge Inner span	490	60.6037	152.817	40.110
I2-6-200	Kalix bridge Inner span	396	56.4303	140.867	39.168
I2-10-100	Kalix bridge Inner span	519	59.4419	152.286	39.852
IW2-6-100	Kalix bridge Inner span	381	43.4309	143.922	35.894
IW2-6-200	Kalix bridge Inner span	436	57.1502	151.212	39.333
I3-2-100*	Kalix bridge Inner span	463.78	57.3277	151.296	39.374
I3-3-100*	Kalix bridge Inner span	509.78	62.7448	153.775	40.577

F_{Max} is the maximum load the core sample bears, σ_c is the uniaxial compressive strength of the concrete, G_F is the Fracture Energy, calculated using the fib Model Code 2010 (2013), E is the Elastic Modulus of the concrete, calculated using the expression proposed by the Comité Euro-International du Béton and the ENV 1992-1-1 (Eurocode 2).

Table 7: Summary of the results obtained from compression tests over the slab cores

Core tag	Core origin	F_{Max} (kN)	σ_c (MPa)	G_F (Nm/mm^2)	E (GPa)
Slab_TB-1	Slab	425	57.512	151.384	39.416
Slab_TB-2	Slab	435	57.965	151.598	39.519
Slab_TB-3	Slab	385	51.302	148.302	37.943

F_{Max} is the maximum load the core sample bears, σ_c is the uniaxial compressive strength of the concrete, G_F is the Fracture Energy, calculated using the fib Model Code 2010 (2013), E is the Elastic Modulus of the concrete, calculated using the expression proposed by the Comité Euro-International du Béton and the ENV 1992-1-1 (Eurocode 2).

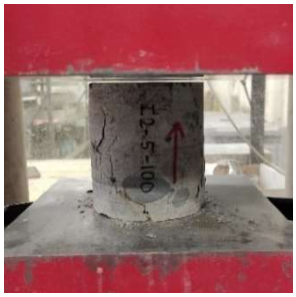

Figure 40: Core sample after compression test (1); load rate of 6.28kN/s

Figure 41: Core sample after compression test (2); load rate of 10kN/s

5.1.2. 3PBT results

In the following Table 8, the geometrical parameters of the cast beams are listed. These parameters will be used for calculating the Fracture Energy of the concrete:

Table 8: Geometrical parameters of beams prepared for the 3PBT

Beam tag	Beam origin	s (mm)	L (mm)	b (mm)	d (mm)	a (mm)	A_{notch} (mm^2)	W (kg)
Ba1_1	Cast	400	600	78.3	128.56	42.85	6710.832	14.22
Ba1_7	Cast	375	480	75	125	41.67	6249.75	10.595
Ba1_Uknown	Cast	400	600	77.50	127.50	42.50	6587.50	13.96

s is the span (distance between supports), L is the length of the beam, b is the width of the beam, d is the depth of the beam. A_{notch} is the area of the beam at the notch section. The notch depth is desired to be 1/3 of the depth of the beam.

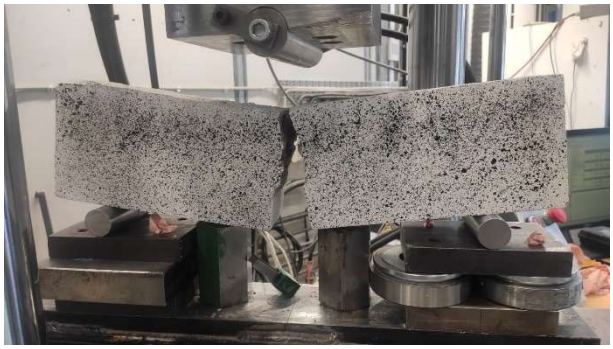

Figure 42: Cast concrete beam after 3PBT

In the following Table 9, the results from 3PBT are listed:

Table 9: Summary of the results obtained from 3PBT

Beam tag	Beam origin	F_{Max} (kN)	δ_{Max} (µm)	COD_{Max} (µm)	$G_{F,exp}$ (Nm/mm^2)	$G_{F,theo}$ (Nm/mm^2)
Ba1_1	Cast	4.964	*	2576	113.834	119.309
Ba1_7	Cast	5.393	3959	2634	108.496	118.079
Ba1_10	Cast	4.456	3455	2937	114.847	120.952

F_{Max} is the maximum load the beam bears, COD_{Max} is the maximum Crack opening displacement registered by the gage, $G_{F,exp}$ is the area under the curve load – deflection (shown in Figure 6), $G_{F,theo}$ is the theoretical Fracture Energy, calculated with equation 3.2.1.5, δ_{Max} is the maximum deflection.
* For Ba1_1, the deflection was not measured. Thus, δ_{Max} is not among the recorded data.

The Load (kN) – COD (μm) curves for the three tested beams are plotted, as shown in the following figures:

Ba1_1:

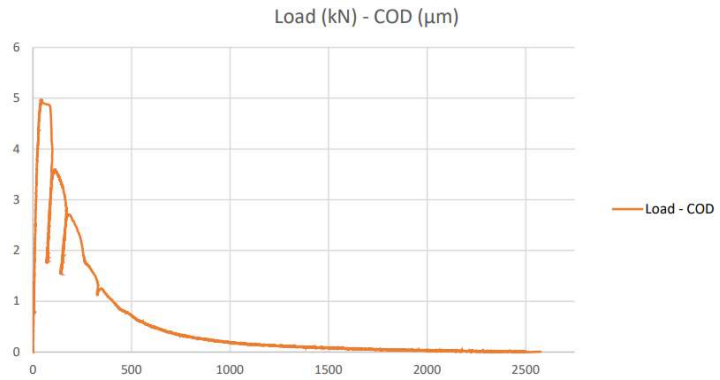

Figure 43: Load – Crack Opening Displacement curve for Ba1_1

Ba1_7:

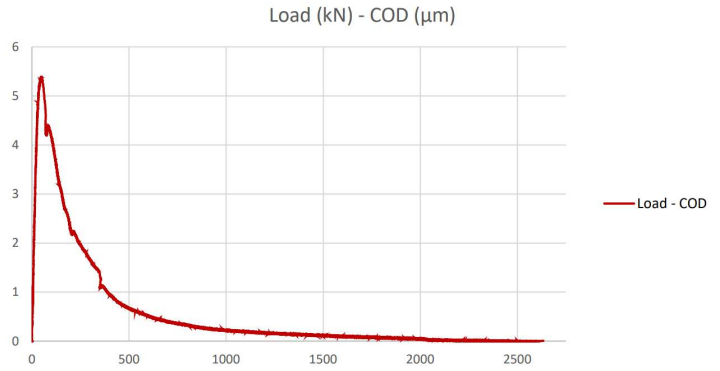

Figure 44: Load – Crack Opening Displacement curve for Ba1_7

Ba1_10:

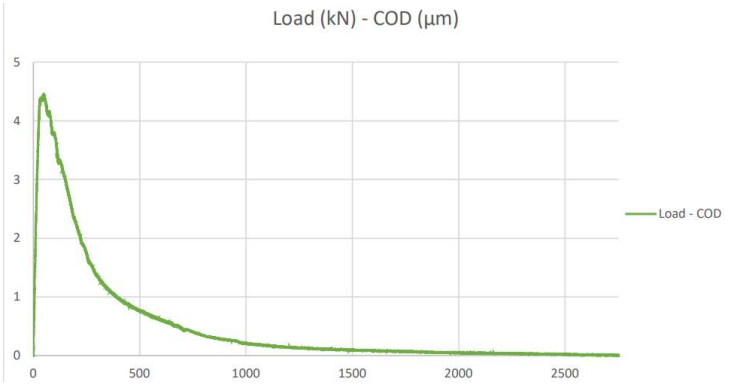

Figure 45: Load – Crack Opening Displacement curve for Ba1_10

5.1.3. Tensile test results

The tests were carried out with the following specifications: Notch depth of 15mm (in radius; 30mm in diameter), so that the smaller diameter was 70mm. This notch was cut at the mid-height of the core sample. The length of the cores varied from one another. In order to fix the core sample in the machine and apply the tensile strength, two steel plates were glued at the top and at the bottom of the cylinders. For that purpose, the ends of each core sample, as well as the steel plates, were first polished and then cleaned using acetone and isopropanol (in that order). The used glue was the two-phase X60-NP glue, consisting of 2 components (A and B) that need to be mixed in the correct proportions. The displacement rate was 0.05µm/s. With the purpose of accelerating the tests, the displacement rate is modified, and when the load reaches 0.5kN, the displacement rate changes to 0.1µm/s.

Nevertheless, there were glue failures at the top surface, possibly caused by a not good polishing/cleaning of the core surfaces or the loading plates. In order to fix this problem, there were 2 different possibilities. First, the notch could be deeper, so that the transversal area was smaller. Secondly, the specimens could be cut in the ends, so that the specimens were smaller in length. Anyways, the ends needed to be cut, since for regluing them, the previous hardened glue had to be removed. Therefore, the ends were cut, and the specimens were shortened. Additionally, the notch depth was increased to a value of 20mm in radius. Thus, the smaller diameter, where the fracture of the core is intended, was 60mm.

In the following Table 10, the geometrical parameters of the core samples that were prepared specifically for carrying out tensile tests are listed:

Table 10: Geometrical parameters of core samples prepared for tensile tests

Core tag	Core origin	L (mm)	Ø (mm)	$Ø_0$ (mm)	A_{notch} (mm^2)	W (g)
Ba1_100	Cast	100	100	70	3848.451	1849.14
Ba1_150	Cast	150	100	70	3848.451	2773.72

Slab_TB-4_renotched	Slab	170.25	97.13	60.07	2834.035	2996.5
Slab_TB-5_renotched	Slab	164.0	97.13	60.1	2836.866	2886.5
Slab_TB-6_renotched	Slab	131.8	97.38	60.13	2839.699	2320.0
Slab_TB-7_renotched	Slab	134.09	97.5	60.02	2829.319	2368.0
Slab_TB-8_renotched	Slab	133.29	97.5	60.22	2848.206	2338.5
Slab_TB-9_renotched	Slab	133.92	97.5	60.05	2832.148	2356.0
Slab_TB-10_renotched	Slab	136.15	97.25	60.05	2832.148	2396.0
Slab_TB-11_renotched	Slab	124.86	97.0	60.16	2842.533	2197.5

L is the length of the core sample; $\emptyset$ is the initial diameter of the core sample, outside the notch; $\emptyset_0$ is the diameter of the core sample at the notch section. These 3 parameters are obtained from the arithmetic mean of 4 measurements taken. A_{notch} is the cross-section area of the core sample at the notch section. W is the weight of the core sample.

In Table 11, the results obtained from the tensile tests are listed:

Table 11: Summary of the results obtained from tensile tests

Core tag	Core origin	F_{Max} (kN)	σ_{Max} (MPa)	G_F (Nm/mm^2)	ω_{Max} (μm)	δ_{Max} (μm)
Ba1_100	Cast	The sample failed before the testing was completed.				
Ba1_150	Cast	12.246	3.182	131.942	493.238	501.363
Slab_TB-4_renotched	Slab	8.85	3.123	112.744	361.311	367.554
Slab_TB-5_renotched	Slab	8.986	3.167	148.664	339.548	351.063
Slab_TB-6_renotched	Slab	Glue failure. No results taken.				
Slab_TB-7_renotched	Slab	7.595	2.684	151.608	241.828	255.376
Slab_TB-8_renotched	Slab	Glue failure. No results taken.				
Slab_TB-9_renotched	Slab	8.818	3.113	117.471	212.280	222.768
Slab_TB-10_renotched	Slab	7.651	2.701	118.105	247.365	255.171
Slab_TB-11_renotched	Slab	8.466	2.978	100.751	211.305	218.486

F_{Max} is the maximum load applied to the core sample, σ_{Max} is the uniaxial tensile strength of the core samples, calculated by dividing F_{Max}/A_{notch}. G_F is the Fracture Energy obtained as the area under the Stress – Crack Width curve. ω_{Max} is the maximum crack width, and δ_{Max} is the maximum displacement.

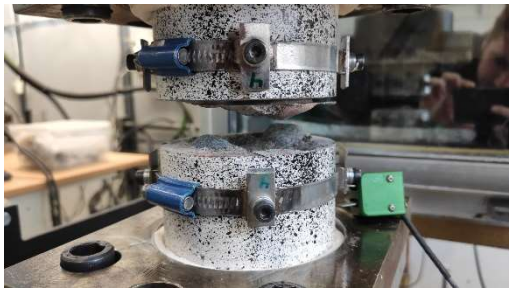

Figure 46: Core sample after tensile test is performed (1)

Figure 47: Core sample after tensile test is performed (2)

Both Load (kN) – Displacement (µm) and Stress (MPa) – Crack Width (µm) curves will be represented for each of the specimens. The value of Fracture Energy (G_F) is the area under the Stress-Crack width curve. Note that this curve starts at the highest stress applied or, in other words, the highest load applied, and ends when the specimen is fractured.

Ba1_150:

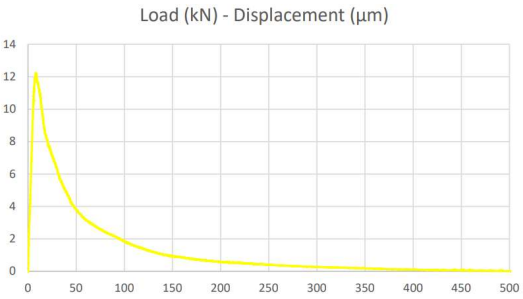

Figure 48: Load - Displacement curve for Ba1_150

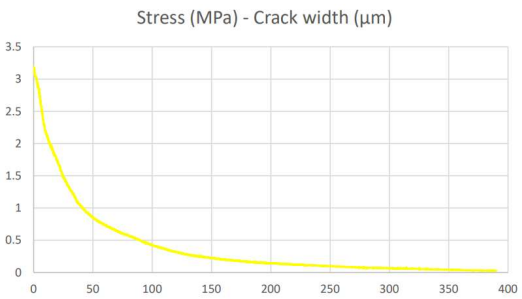

Figure 49: Stress - Crack width curve for Ba1_150

Slab_TB-4_Renotched:

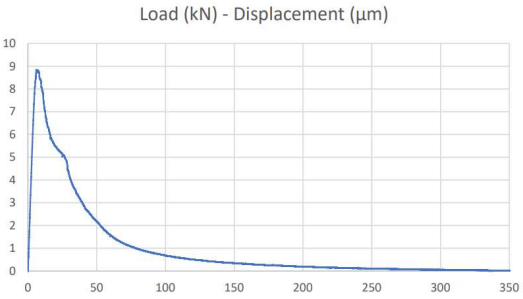

Figure 50: Load - Displacement curve for Slab_TB-4_Renotched

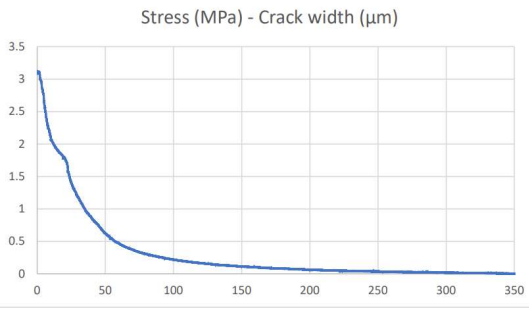

Figure 51: Stress - Crack width curve for Slab_TB-4_Renotched

Slab_TB-5_Renotched:

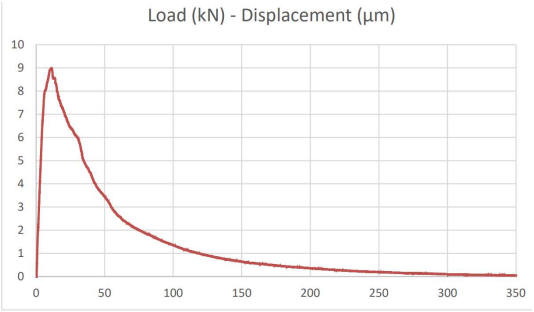

Figure 52: Load - Displacement curve for Slab_TB-5_Renotched

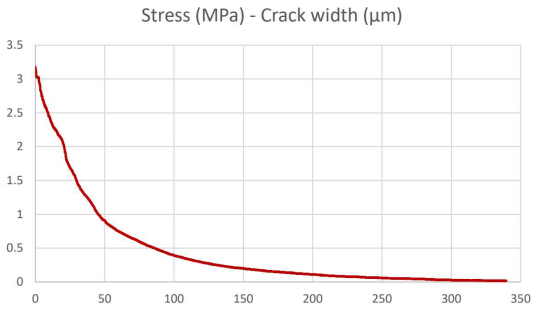

Figure 53: Stress - Crack width curve for Slab_TB-5_Renotched

Slab_TB-6_Renotched: Suffered a glue failure. Thus, the curves will not be represented since they would not provide useful values.

Slab_TB-7_Renotched:

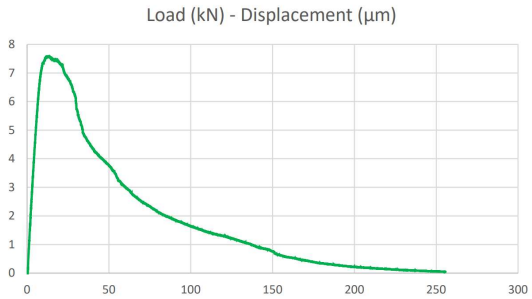

Figure 54: Load - Displacement curve for Slab_TB-7_Renotched

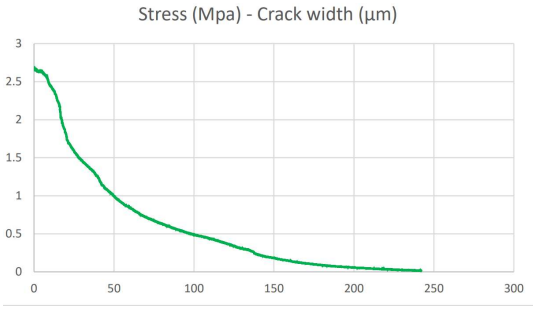

Figure 55: Stress - Crack width curve for Slab_TB-7_Renotched

Slab_TB-8_Renotched: Suffered a glue failure. Thus, the curves will not be represented since they would not provide useful values.

Slab_TB-9_Renotched:

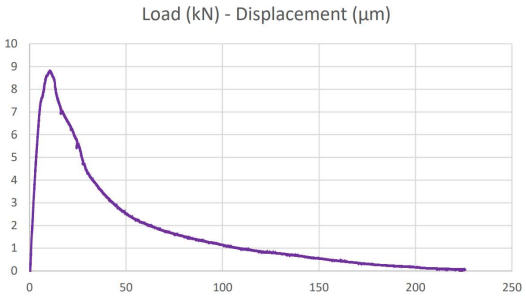

Figure 56: Load - Displacement curve for Slab_TB-9_Renotched

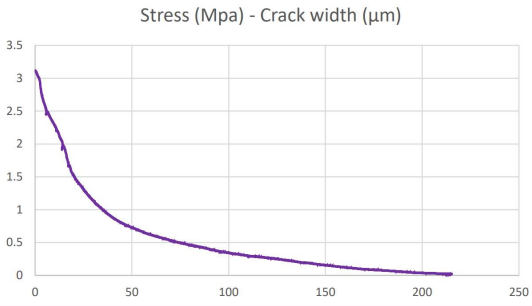

Figure 57: Stress - Crack width curve for Slab_TB-9_Renotched

Slab_TB-10_Renotched:

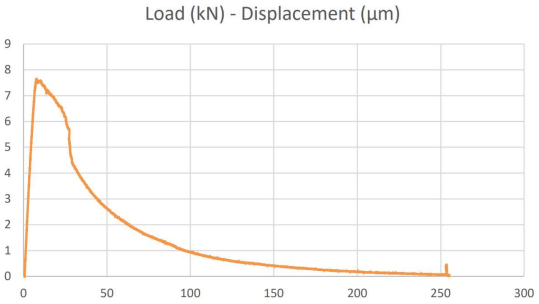

Figure 58: Load - Displacement curve for Slab_TB10_Renotched

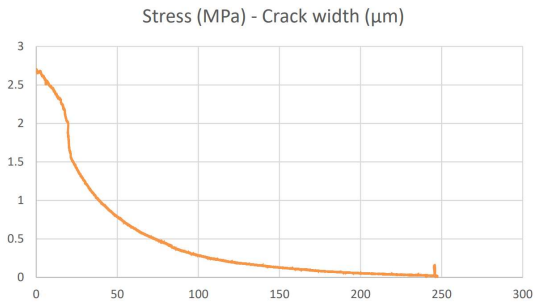

Figure 59: Stress - Crack width curve for Slab_TB-10_Renotched

Slab_TB-11_Renotched:

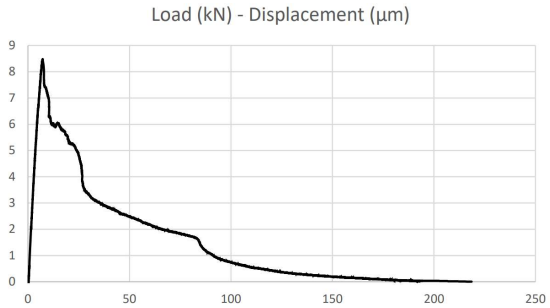

Figure 60: Load - Displacement curve for Slab_TB11_Renotched

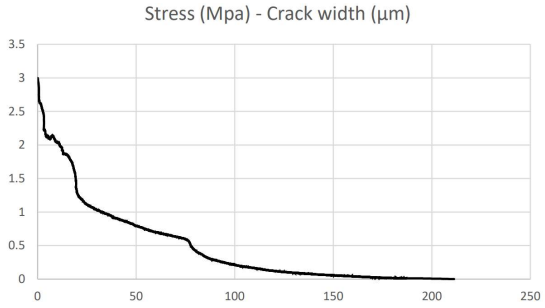

Figure 61: Stress - Crack width curve for Slab_TB-11_Renotched

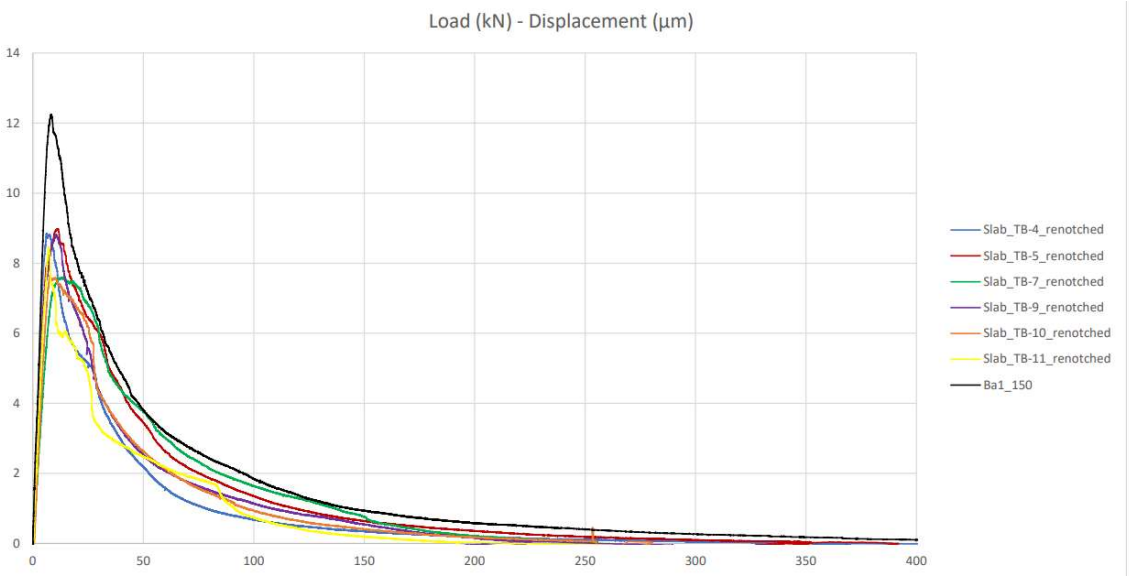

Figure 62: Load - Displacement curves of tested cylinders/cores

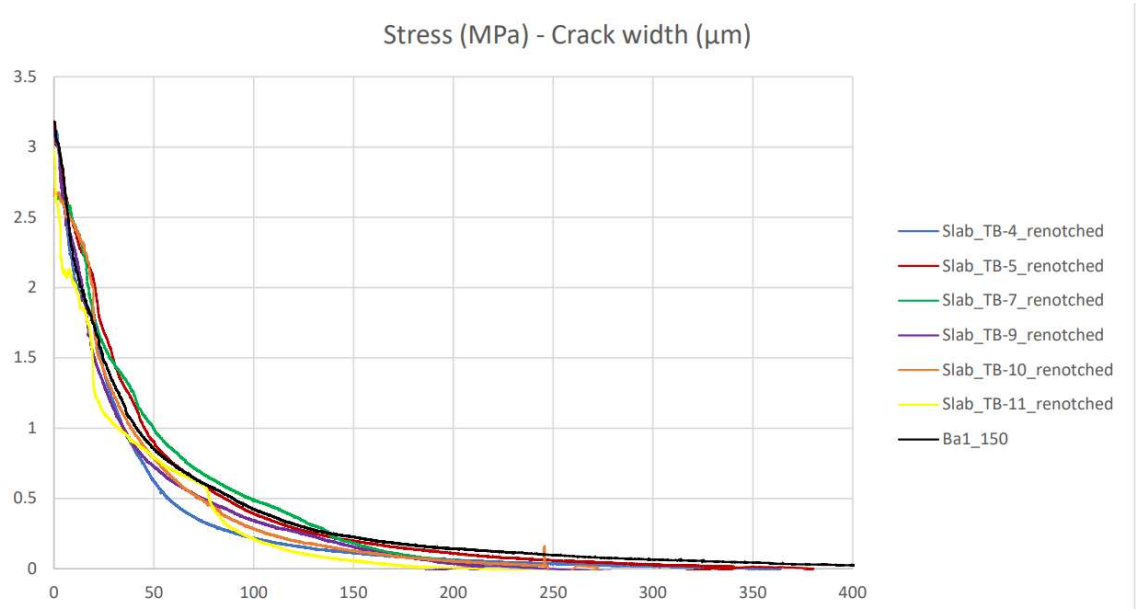

Figure 63: Stress - Crack width curves of tested cylinders/cores

Figure 62 And Figure 63 show the comparison between the results obtained from tensile tests. It needs to be mentioned that Ba1_150 bears a higher maximum load than the rest of the tested cores. This is because the area at the notch section is greater than the rest. When looking at Figure 63, the stress values for all the tested cylinders and cores are really similar, which implies that the Fracture Energy obtained is similar as well. Nevertheless, it can be seen that the Fracture Energy values of Slab_TB-5_renotched and Slab_TB-7_renotched are slightly higher than the rest.

Based on the results obtained for the different samples, it was observed that the length of the cores and cylinders have influence on the success of the experiments. For longer cores a deeper notch needed to be used in order to avoid their failure at the surfaces in contact with the glue.

5.2. Finite Element Modeling

Concrete models and test results through the realization of FEM are presented in this section. Three different models are created with ATENA Science V.5.9. software. They are all constitutive models of concrete, whose mechanical properties are defined prior to running the tests. For each model, these properties were different, depending on the precedence of the sample, but for all of them, the defined concrete material is based on EuroCode2.

5.2.1. Concrete core

A 3D concrete core model is developed (see Figure 64). For that purpose, the cylinder creator tool is used, with a base diameter of 100mm. The concrete strength class, the Young Modulus and the Poisson's ratio depend on the study case assessed.

When creating the mesh, the finite element type used was tetrahedra with 4 nodes, and the mesh size applied was 0.01m (see Figure 65). In order to obtain precise results, it's better to create the finest mesh as possible.

The load is applied at the top end of the cylinder. The applied load rate consists in a distributed load with the value of 3.92kN/m^2 per step. Since the concrete cores are modelled just to carry out compression tests, this load rate follows the vertical direction. The obtained results from this model are, basically, the maximum applied load over the core and the maximum stress the core can bear. That data will be used, just like in Section 5.1.1, to obtain values of Fracture Energy.

Moreover, boundary conditions need to be applied. For the bottom base, the displacement on y-axis (vertical) and x-axis (first horizontal axis) is fixed, so the movement is not allowed in those directions. Regarding the upper end, the displacement on x-axis and z-axis (first and second horizontal axis) is fixed, but the displacement in the vertical axis is free. Therefore, when applying the compression loads on the core, the displacement would only happen in the vertical direction.

Four different concrete core models have been developed using FEM. The first two models are from the first study case (trough bridge), and the other two from the second study case (Kalix bridge).

For the first study case, a model of 162mm and a model of 164mm long have been developed, and for the second study case, models of 100mm and 200mm are created. The lengths of the cores developed in FEM are similar to the lengths of the cores presented in Section 5.1.1.

As mentioned previously, the concrete strength class depends on the study case as well. Thus, trough bridge study case presents a concrete strength class of 45/55, while Kalix bridge study case has a concrete strength class of 40/50.

In the following Table 12, the geometrical parameters of the developed finite element models are presented:

Table 12: Geometrical parameters of the developed FEM concrete cores

Core tag	L (mm)	Ø (mm)	A (mm^2)	Load per step (kN/m^2)
TB_162	162	100	7853.982	3.92
TB_164	164			
Kalix_100	100			
Kalix_200	200			

L is the length of the cores, Ø is the diameter of the cores, A is the cross-section area of the cores. The diameter and the area of the cores are the same for all of them, as well as the load per step.

Compression tests are performed over these cores. Therefore, only the maximum load values obtained from the FEM are of interest. With those values, the uniaxial compressive strength, the fracture energy and the Young Modulus can be assessed.

In the following Table 13, the obtained results for maximum load and the calculated mechanical properties of the models are shown:

Table 13: Obtained results using FEM for the concrete cores

Core tag	F_{Max} (kN)	σ_c (MPa)	G_F (Nm/mm^2)	E (GPa)
TB_162	372.26	47.398	146.204	36.955
TB_164	372.303	47.390	146.200	36.953
Kalix_100	336.728	42.862	143.581	35.737
Kalix_200	336.864	42.879	143.591	35.741

F_{Max} is the maximum load the core sample bears, σ_c is the uniaxial compressive strength of the concrete, G_F is the Fracture Energy, calculated using the fib Model Code 2010 (2013), E is the Elastic Modulus of the concrete, calculated using the expression proposed by the Comité Euro-International du Béton and the ENV 1992-1-1 (Eurocode 2).

The mean value of the Fracture Energy values for the concrete cores developed with FEM for the first study case is 146.202 Nm/mm^2. In Section 5.1.1, 3 concrete cores of about 162mm and 164mm were tested and presented a mean value for Fracture Energy of 150.428 Nm/mm^2. The values are really similar. Therefore, it can be stated that the developed model with the FEM software is accurate, with an error estimation of 2.81%.

On the other hand, the Fracture Energy value for the finite element developed concrete core of 100mm long was 143.581 Nm/mm^2, while the Fracture Energy mean value of the concrete cores extracted in Kalix (presented in Section 5.1.1) was 152.654 Nm/mm^2 for the Outer span, and 150.819 Nm/mm^2 for the Inner span. The values are similar, but not 100% accurate. The error estimation for the Outer span is 5.94%, and 4.8% for the Inner span.

Finally, the Fracture Energy value obtained through FEM for the 200mm long concrete core was 143.591 Nm/mm^2. In Section 5.1.1, for the Outer span the Fracture Energy mean value was 150.991 Nm/mm^2, and for the Inner span was 146.04 Nm/mm^2. In this case the error estimation for both outer and inner span is lower, obtaining results in error of 4.9% and 1.68%, respectively.

It can be stated that the developed Finite Element Model of the concrete core is accurate enough to predict the Fracture Energy values of both study cases, since in any case, the error estimation is higher than the 6%.

The following Figure 64 and Figure 65 show an example of the developed concrete core with FEM. More precisely, it is the 100mm long concrete core.

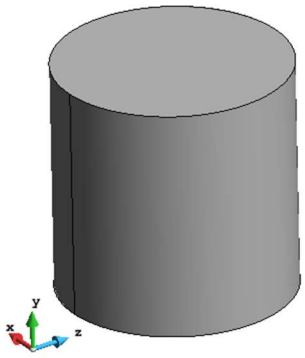

Figure 64: Example of concrete core created with FEM

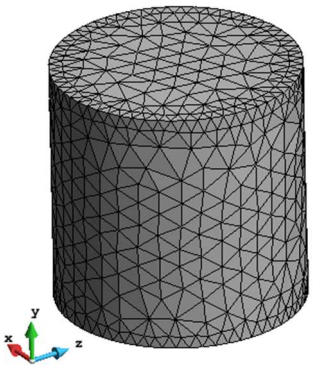

Figure 65: Mesh layout of example of concrete core

In Appendix 2, front, top and isometric views of one of the developed models are displayed.

5.2.2. Notched beam

A 3D concrete beam model is developed as well (see Figure 68), in order to simulate a 3PBT. It is essential to include the notch to the model, so that it is similar to the one test in laboratory. Since these beams were just part of the First study case (trough bridge case), only the concrete from this study case is included in the FEM software. Therefore, its strength class is 45/55, and the density is 2300kg/m^3.

This model has its particularities. Three plates need to be created: two of them at the bottom of the beam, and one at the top. The load is applied right at the center of the top plate. On the other hand, the bottom plates serve as supports. Therefore, what is measured is the maximum opening displacement. The rest of parameters needed to obtain values of Fracture Energy are input in the program.

The mesh size and finite element type used is the same as in the previous model: Tetrahedral elements with 4 nodes, and a mesh size of 0.01m. Again, the finer the mesh is, more accurate results are obtained (see Figure 69).

The boundary conditions for this model include the fixed displacement of some parts, as well as the contact between the beam and the plates. The bottom plates have a fixed contact with surface to the beam, so that the plates move together with the beam. On the other hand, the top plate has a contact surface, but it is not fixed. One of the bottom plates has a fixed displacement of zero in all the three axes, so that the movement is impeded in the three directions. The other bottom plate does not need the same displacement boundary conditions since both plates are fixed to the beam. The top plate is fixed in such way that it can nor rotate.

In the following Table 14, the geometrical parameters of finite element models of a beam are listed. These parameters will be used later for calculating the Fracture Energy:

Table 14: Geometrical parameters of the developed FEM beam

Beam tag	s (mm)	L (mm)	b (mm)	d (mm)	a (mm)	A_{notch} (mm^2)	W (kg)
TB-Beam_1	400	600	75	125	41.67	6250	12.938
TB-Beam_2	375	400	75	125	41.67	6250	8.625

s is the span (distance between supports), L is the length of the beam, b is the width of the beam, d is the depth of the beam. A_{notch} is the area of the beam at the notch section, W is the total weight of the beam. The notch depth is desired to be 1/3 of the depth of the beam.

In the following Table 15, the results obtained using the FEM software are listed:

Table 15: Obtained results for the beam from FEM

Beam tag	F_{Max} (kN)	δ_{Max} (µm)	COD_{Max} (µm)	$G_{F,exp}$ (Nm/mm^2)	$G_{F,theo}$ (Nm/mm^2)
TB-Beam_1	4.729	*	12035.9	-	-
TB-Beam_2	4.368	*	11281.6	-	-

F_{Max} is the maximum load the beam bears, COD_{Max} is the maximum Crack opening displacement registered by the gage, $G_{F,exp}$ is the area under the curve load – deflection (shown in Figure 6), $G_{F,theo}$ is the theoretical Fracture Energy, calculated with equation 3.2.1.5, δ_{Max} is the maximum deflection.
* The deflection was not measured. Thus, δ_{Max} is not among the recorded data.

The Load (kN) – COD (µm) curves for both finite element models are represented. The value of Fracture Energy (G_F) is the area under the Stress-Crack width curve. Note that this curve starts at the highest stress applied or, in other words, the highest load applied, and ends when the specimen is fractured.

TB-Beam_1:

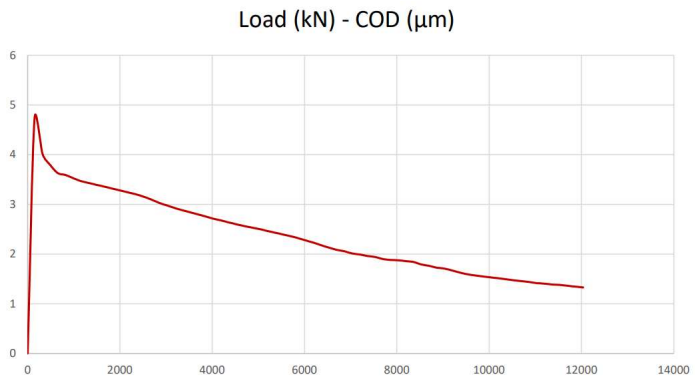

Figure 66: Load – Crack Opening Displacement curve for TB-Beam_1

TB-Beam_2:

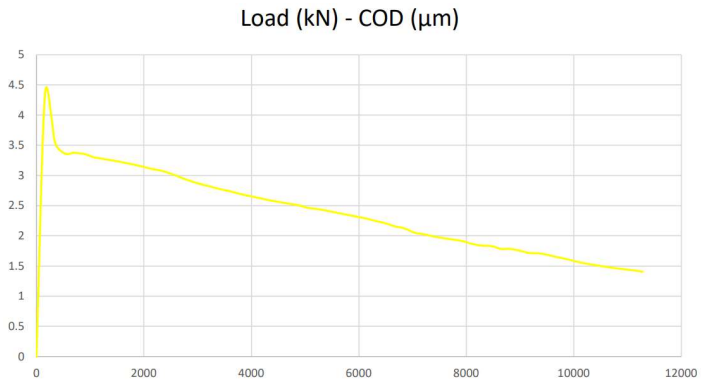

Figure 67: Load – Crack Opening Displacement curve for TB-Beam_2

As it can be seen, the values obtained with FEM are completely different to the ones presented in Section 5.1.2. Therefore, the developed models with the FEM software were not adequate. The Fracture Energy values are not presented in Table 15 since they are not accurate. The cast beams in Section 5.1.2 presented a mean value for COD of 2916.67µm, while the ones presented in this Section 5.2.2 supposedly fail when COD reaches 12000µm.

New models need to be developed in FEM in order to obtain more accurate results, and so that the behavior of both case studies can be predicted. The following Figure 68 and Figure 69 show the developed Finite Element Model of the beam.

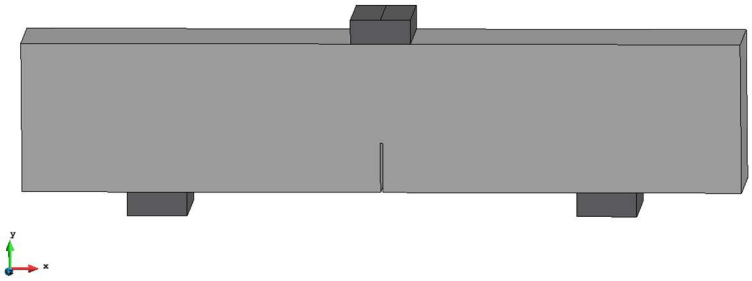

Figure 68: Example of notched concrete beam developed with FEM

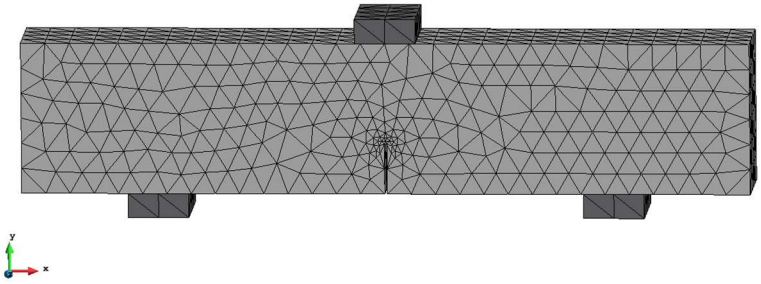

Figure 69: Mesh layout for the example of notched concrete beam

In Appendix 3, front, top and isometric views of the whole model (are included, as well as an isometric view of the and an isometric view of a plate.

5.2.3. Notched concrete core

This model (see Figure 80) is a variation of the first one (Section 5.2.1). It is a 100mm diameter concrete core as well but, in this case, a notch is created at the middle of the cylinder. In order to develop this model, three different cylinders are created, and fixed one to each other through boundary conditions (top cylinder is fixed to middle cylinder; middle cylinder is fixed to both top and bottom cylinder). In this case, only cores from the second study case (Kalix bridge) are developed. Therefore, the concrete strength class used when modelling the core in FEM is 40/50. Again, the concrete strength class will affect directly on the obtained values.

The finite element type is, again, tetrahedral element with 4 nodes, and the mesh size is 0.01m. The middle cylinder is divided in portions so that the mesh type can be applied correctly to the model, and the results to be accurate (see Figure 81).

This notched concrete core model is created to simulate tensile tests. Therefore, the maximum load applied is measured, as well as the load – displacement and stress – crack width curves. Nevertheless, a displacement per step of 0.1mm/step is used in this model, instead of the usual load per step, in order to obtain the displacement values required.

About the boundary conditions, they are the same as the ones explained for the concrete core (Section 5.2.1), with the only particularity that, in this case, the top and bottom surfaces of the middle cylinder have to be fixed to the bottom surface of the upper cylinder and the top surface of the bottom cylinder, respectively.

In the following Table 16, the geometrical parameters of the developed finite element models are presented:

Table 16: Geometrical parameters of the developed FEM concrete beams

Core tag	L (mm)	Ø (mm)	$Ø_0$ (mm)	A_{notch} (mm^2)
Kalix_150-70	150	70	100	3848.451
Kalix_200-70	200	70	100	3848.451
Kalix_170-60	170	60	100	2827.433
Kalix_130-60	130	60	100	2827.433

L is the length of the core sample; Ø is the initial diameter of the core sample, outside the notch; $Ø_0$ is the diameter of the core sample at the notch section. A_{notch} is the cross-section area of the core sample at the notch section.

In the following Table 17, the obtained results for Maximum load and the calculated mechanical properties of the models are shown:

Table 17: Obtained results using FEM for the concrete beams

Core tag	F_{Max} (kN)	σ_{Max} (MPa)	G_F (Nm/mm^2)	ω_{Max} (μm)	δ_{Max} (μm)
Kalix_150-70	9.468	2.46	90.647	98.972	107.04
Kalix_200-70	10.14	2.635	60.875	55.526	65.533
Kalix_170-60	7.486	2.648	137.517	335.981	343.546
Kalix_130-60	7.4978	2.652	119.51	203.433	210.051

F_{Max} is the maximum load applied to the core sample, σ_{Max} is the uniaxial tensile strength of the core samples, calculated by dividing F_{Max}/A_{not} . G_F is the Fracture Energy obtained as the area under the Stress – Crack Width curve. ω_{Max} is the maximum crack width, and δ_{Max} is the maximum displacement.

The first two finite element models (Kalix_150-70 and Kalix_200-70) were not completely developed. Thus, the obtained values for Fracture Energy, ω_{Max} and δ_{Max} are not the real ones, and the real values would be higher than the presented values. Looking at the rest of the results, the Fracture Energy values should be around 140 Nm/mm^2, higher than the ones with a cross-section area at the notch of 60mm.

In Section 5.1.3, values for Fracture Energy were presented, obtained through tensile tests carried out in laboratory. For the cores that were, more or less, 170mm long, the mean Fracture Energy value obtained was 130.704 Nm/mm^2, while the obtained value through FEM is 137.517 Nm/mm^2. The estimated error committed is 4.95%, which is low.

The mean Fracture Energy value of the cores in Section 5.1.3. that were about 130mm long was 121.98 Nm/mm^2, and the obtained value using FEM is 119.51 Nm/mm^2. Therefore, the estimated error is 2.07%, which is very low.

Once the Fracture Energy values obtained analytically and experimentally are evaluated and compared, it can be said that the developed Finite Element Models are accurate enough, since the estimated error committed is never higher than the 5%. Nevertheless, some of the data of the FEM were not evaluated, and it needs to be analyzed in order to state that the FEM is good.

Both Load (kN) – Displacement (µm) and Stress (MPa) – Crack Width (µm) curves will be represented for each of the models. The value of Fracture Energy (G_F) is the area under the Stress-Crack width curve. Note that this curve starts at the highest stress applied or, in other words, the highest load applied, and ends when the specimen is fractured.

Kalix_150-70:

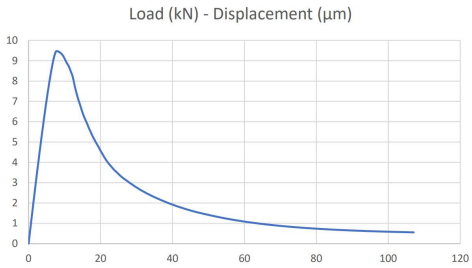

Figure 70: Load - Displacement curve for Kalix_150-70

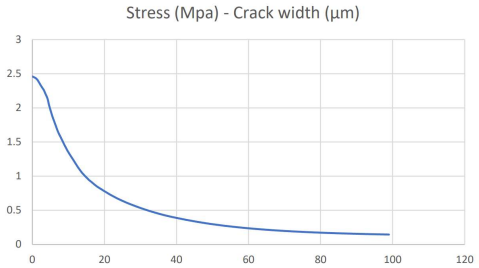

Figure 71: Stress - Crack width curve for Kalix_150-70

Kalix_200-70:

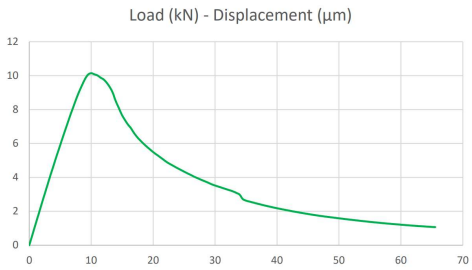

Figure 72: Load - Displacement curve for Kalix_200-70

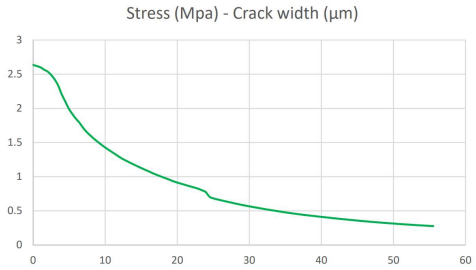

Figure 73: Stress - Crack width curve for Kalix_200-70

Kalix_170-60:

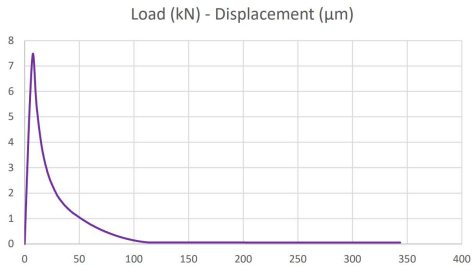

Figure 74: Load - Displacement curve for Kalix_170-60

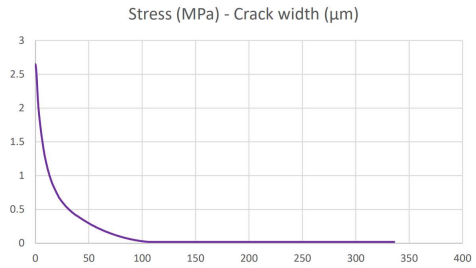

Figure 75: Stress - Crack width curve for Kalix_170-60

Kalix_130-60:

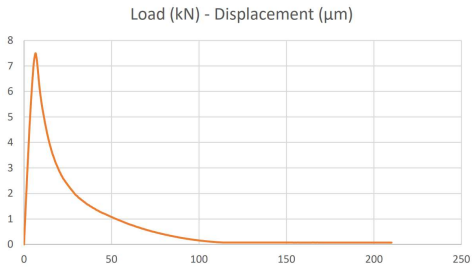

Figure 76: Load - Displacement curve for Kalix_130-60

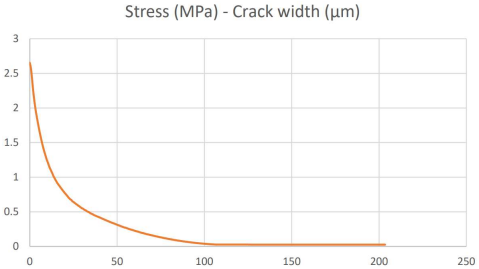

Figure 71: Stress - Crack width curve for Kalix_130-60

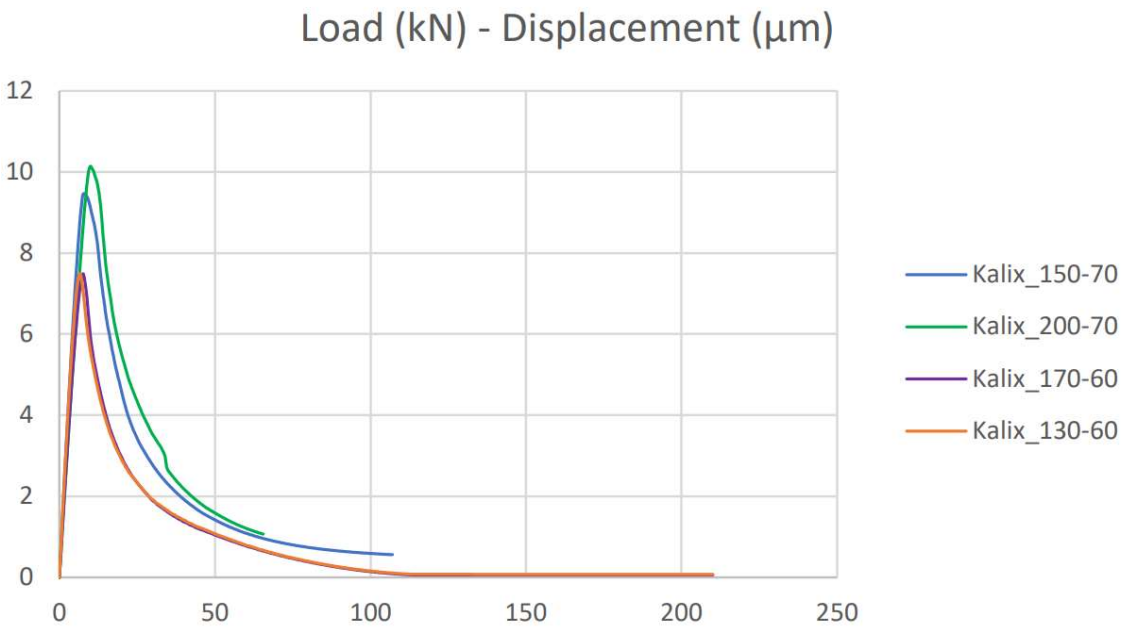

Figure 78: Load - Displacement curves of finite element models

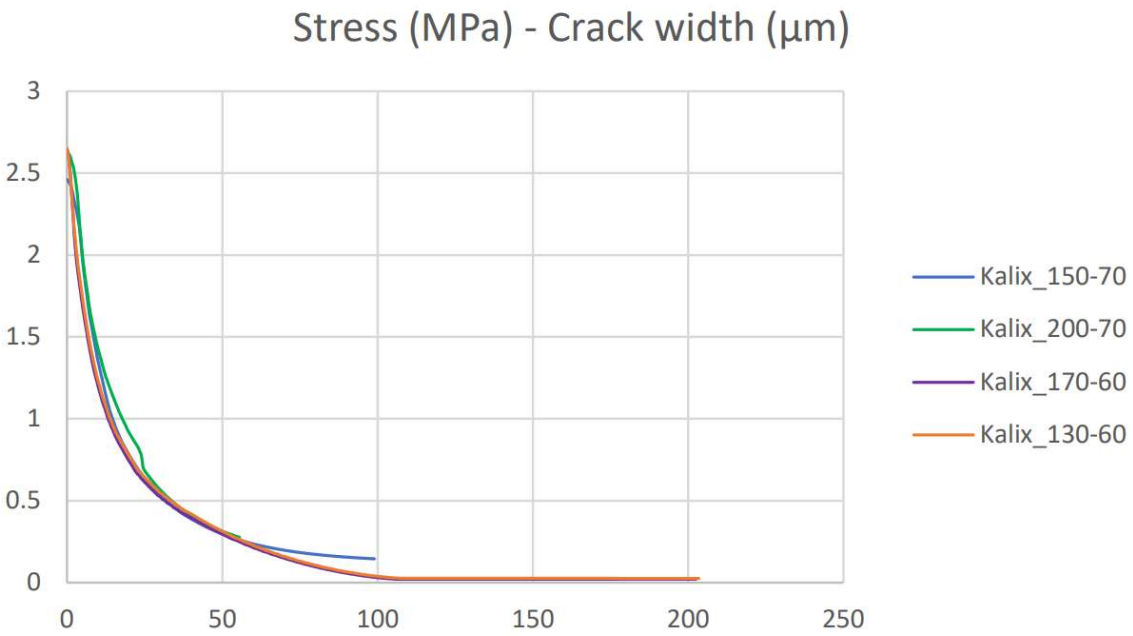

Figure 79: Stress - Crack width curves of the finite element models

The following Figure 80 and Figure 81 show an example of the developed notched concrete core with FEM. More precisely, it is the 100mm long notched concrete core.

Figure 80: Example of notched concrete core developed with FEM

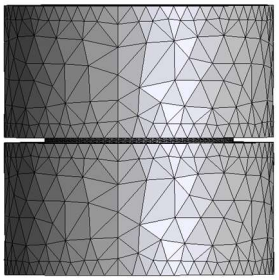

Figure 81: Mesh layout for example of notched concrete core

In Appendix 4, front, top, and isometric views of the whole example model are included, as well as an isometric view of the top/bottom cylinder and an isometric view of the middle cylinder.

6. Conclusions and future work

Experimental and numerical evaluations over concrete samples have been carried out. Throughout this study, some of the mechanical properties of the concrete from two different study cases have been assessed. Values of Young Modulus, tensile and compressive strength, and fracture energy have been obtained through empirical tests over samples from both the Trough bridge and the Kalix bridge.

The mean Uniaxial tensile strength (σ_t) of the Kalix bridge was 3.182MPa, while the one from the Trough bridge was 2.961MPa. The mean Uniaxial compressive strength (σ_c) of the Kalix bridge was 59.39MPa for the Outer span and 56.73MPa for the Inner span, while the one from the Trough Bridge was 55.59MPa. σ_t obtained with FEM was 2.6MPa in the Kalix model. σ_c obtained with FEM was 47.394MPa in the Trough bridge model, and 42.87MPa in the Kalix model.

6.1. Research questions

RQ1: does the proposed methodology for the evaluation of concrete fracture energy provide adequate results?

Fracture Energy results of both numerical and experimental have been compared in Section 5.2. These results have proven that the developed Finite Element Models carried out were accurate. The highest estimated error committed was less than 6%, and the lowest one was 1.68%. However, Finite Element Models can be slightly improved in the future, in order to obtain more precise results for Fracture Energy.

RQ2: what are the parameters that influence the results of the fracture energy obtained through the proposed methodology?

Based on the results obtained for the different samples, it was observed that the length of the cores and cylinders have influence on the success of the experiments. For longer cores a deeper notch needed to be used in order to avoid their failure at the surfaces in contact with the glue.

6.2. Future research

In order to improve the proposed method, more tests can be performed over samples from the cast in laboratory Trough Bridge, so that the mechanical properties of the concrete can be obtained. With a larger number of samples tested, the values of the properties of the material are more accurate.

In addition, numerical parametric studies can be performed, using the Finite Element Models developed. This can help to guide the execution of future tests, and to evaluate the influence of additional parameters.

7. References

ACI Committee 228--Nondestructive Testing of Concrete. (2003). In-place methods to estimate concrete strength. American Concrete Institute.

ACI Committee 363. (1984). State-of-the-art Report on High-strength Concrete (ACI 363R-84). American Concrete Institute.

Architectural Institute of Japan, "Standard for Structural Calculation of Reinforced Concrete Structures," Chapter 2, AIJ, 1985, pp. 8-11.

ASTM, C. (2002). 805-02,". *Standard test method for rebound number of hardened concrete," USA: ASTM*.

Badawy, R., El-Mowafy, O., & Tam, L. E. (2016). Fracture toughness of chairside CAD/CAM materials–Alternative loading approach for compact tension test. *Dental Materials*, *32*(7), 847-852.

Barros, J. A., & Sena-Cruz, J. (2001). Fracture energy of steel fiber-reinforced concrete.

Bažant, Z. P., & Prat, P. C. (1988). Effect of Temperature and Humidity on Fracture Energy. *ACI Materials Journal*.

Bažant, Z. P. (1996). Analysis of work-of-fracture method for measuring fracture energy of concrete. *Journal of Engineering Mechanics*, *122*(2), 138-144.

Bazant, Z. P., & Planas, J. (2019). *Fracture and size effect in concrete and other quasibrittle materials*. Routledge.

Brühwiler, E., & Wittmann, F. H. (1990). The wedge splitting test, a new method of performing stable fracture mechanics tests. *Engineering fracture mechanics*, *35*(1-3), 117-125.

Code, C. F. M. (1990). Biulletin D'Information, No. 213/214. *CEB Comite Euro-International du Beton*.

Code, C. F. M. (1993). Comité euro-international du béton. *Bulletin d'information*, *213*, 214.

Comité Euro-International du Béton, "High-Performance Concrete, Recommended Extensions to the Model Code 90—Research Needs," CEB Bulletin d'Information, No. 228, 1995, 46 pp

Duan, K., Hu, X., & Wittmann, F. H. (2003). Boundary effect on concrete fracture and non-constant fracture energy distribution. *Engineering Fracture Mechanics*, *70*(16), 2257-2268.

Duan, K., Hu, X., & Wittmann, F. H. (2007). Size effect on specific fracture energy of concrete. *Engineering Fracture Mechanics*, *74*(1-2), 87-96.

Elices, M., Rocco, C., & Roselló, C. (2009). Cohesive crack modelling of a simple concrete: Experimental and numerical results. *Engineering Fracture Mechanics*, *76*(10), 1398-1410.

En, B. S. (2007). 14651,"Test method for metallic fibre concrete—Measuring the flexural tensile strength (Limit of proportionality (LOP), residual). *British Standards Institution, London, UK*.

ENV 1992-1-1, "Eurocode 2. Design of Concrete Structures—Part 1: General Rules and Rules for Buildings," 2004, 225 pp.

Evans, R. H., & Marathe, M. S. (1968). Microcracking and stress-strain curves for concrete in tension. *Matériaux et Construction*, *1*(1), 61-64.

fib Model Code 2010 (2013). fib Model Code 2010 for Concrete Structures. International Federation for Structural Concrete. Berlin: Ernst & Sohn, 2013, 402 p.

Golewski, G. L. (2019). Measurement of fracture mechanics parameters of concrete containing fly ash thanks to use of Digital Image Correlation (DIC) method. *Measurement*, *135*, 96-105.

Guinea, G. V., Planas, J., & Elices, M. (1992). Measurement of the fracture energy using three-point bend tests: Part 1—Influence of experimental procedures. *Materials and Structures*, *25*(4), 212-218.

Hillerborg, A. (1985). The theoretical basis of a method to determine the fracture energyG F of concrete. *Materials and structures*, *18*(4), 291-296.

Hu, X. Z., & Wittmann, F. H. (1992). Fracture energy and fracture process zone. *Materials and Structures*, *25*(6), 319-326.

Hu, X., & Wittmann, F. (2000). Size effect on toughness induced by crack close to free surface. *Engineering fracture mechanics*, *65*(2-3), 209-221.

Huang, J., & Li, V. C. (1989). A meso-mechanical model of the tensile behaviour of concrete. Part II: modelling of post-peak tension softening behaviour. *Composites*, *20*(4), 370-378.

Hughes, B. P., & Chapman, G. P. (1966). The complete stress-strain curve for concrete in direct tension. *Matls & Structures, Res & Testing/Fr/*.

Ioannides, A. M., & Korovesis, G. T. (1990). Aggregate interlock: a pure-shear load transfer mechanism. *Transportation Research Record*, (1286).

Jueshi, Q., & Hui, L. (1997). Size effect on fracture energy of concrete determined by three-point bending. *Cement and Concrete Research*, *27*(7), 1031-1036.

Kaplan, M. F. (1961, November). Crack propagation and the fracture of concrete. In *Journal Proceedings* (Vol. 58, No. 11, pp. 591-610).

Kazemi, M. T., Fazileh, F., & Ebrahiminezhad, M. A. (2007). Cohesive crack model and fracture energy of steel-fiber-reinforced-concrete notched cylindrical specimens. *Journal of materials in civil engineering*, *19*(10), 884-890.

Khalilpour, S., BaniAsad, E., & Dehestani, M. (2019). A review on concrete fracture energy and effective parameters. *Cement and Concrete research*, *120*, 294-321.

Komori, K. (2019). *Ductile Fracture in Metal Forming: Modeling and Simulation*. Academic Press.

Kozłowski, M., Kadela, M., & Kukiełka, A. (2015). Fracture energy of foamed concrete based on three-point bending test on notched beams. *Procedia Engineering*, *108*, 349-354.

Linsbauer, H. N., & Tschegg, E. K. (1986). Fracture energy determination of concrete with cube-shaped specimens. *Zement und Beton*, *31*(1), 38-40.

Malvar, L. J., & Warren, G. E. (1988). Fracture energy for three-point-bend tests on single-edge-notched beams. *Experimental mechanics*, *28*(3), 266-272.

Mannocci, F., Sherriff, M., & Watson, T. F. (2001). Three-point bending test of fiber posts. *Journal of Endodontics*, *27*(12), 758-761.

Mihashi, H., Nomura, N., & Niiseki, S. (1991). Influence of aggregate size on fracture process zone of concrete detected with three dimensional acoustic emission technique. *Cement and Concrete Research*, *21*(5), 737-744.

Mindess, S. (1984). The effect of specimen size on the fracture energy of concrete. *Cement and Concrete Research*, *14*(3), 431-436.

Monteiro, P. J., Helene, P. R., & Kang, S. H. (1993). Designing concrete mixtures for strength, elastic modulus and fracture energy. *Materials and Structures*, *26*(8), 443-452.

Nilimaa, J., Nilforoush, R., Bagge, N., & Elfgren, L. (2020). Testing to Failure of a 55-year-old Prestressed Concrete Bridge in Kiruna: Bending, Shear and Punching of Girders and Slab. Fracture Properties of Materials. Test Results, Modelling and Assessment. Final Report BBT 2017-030.

Noguchi, T., Tomosawa, F., Nemati, K. M., Chiaia, B. M., & Fantilli, A. P. (2009). A practical equation for elastic modulus of concrete. *ACI Structural Journal*, *106*(5), 690.

Nordlund, E., Rådberg, G., Sjöberg, J. (2006). Fundamentals of Rock Mechanics. *Test methods, 5*(1), 132-140.

Omerspahic, E., Mattiasson, K., & Enquist, B. (2006). Identification of material hardening parameters by three-point bending of metal sheets. *International Journal of Mechanical Sciences*, *48*(12), 1525-1532.

Peterson, P. E. (1980). Fracture energy of concrete: Method of determination. *Cement and Concrete research*, *10*(1), 79-89.

Petersson, P. E. (1981). *Crack growth and development of fracture zones in plain concrete and similar materials* (No. LUTVDG/TVBM--1006/1-174/(1981)). Lund Inst. of Tech.(Sweden). Div. of Building Materials.

Ren, D., & Houben, L. (2020). Determination of fracture energy of early age concrete through a uniaxial tensile test on an un-notched specimen. *Materials*, *13*(3), 496.

Rusch, H., & Hilsdorf, H. (1963). Deformation characteristics of concrete under axial tension. *Voruntersuchungen, Bericht*, *44*(5), 0.

Shah, S. P. (1990). Size-effect method for determining fracture energy and process zone size of concrete. *Materials and Structures*, *23*(6), 461-465.

Snozzi, L., Gatuingt, F., & Molinari, J. F. (2012). A meso-mechanical model for concrete under dynamic tensile and compressive loading. *International journal of fracture*, *178*(1), 179-194.

Teng, S., Liu, Y., & Lim, T. Y. D. (2014). Determination of fracture energy of ultra high strength concrete. *Engineering Fracture Mechanics*, *131*, 602-615.

Vydra, V., Trtík, K., & Vodák, F. (2012). Size independent fracture energy of concrete. *Construction and Building Materials*, *26*(1), 357-361.

Wagnoner, M. P., Buttlar, W., & Paulino, G. H. (2005). Disk-shaped compact tension test for asphalt concrete fracture. *Experimental mechanics*, *45*(3), 270-277.

Wittmann, F. H., Mihashi, H., & Nomura, N. (1990). Size effect on fracture energy of concrete. *Engineering Fracture Mechanics*, *35*(1-3), 107-115.

Wittmann, F. H., Roelfstra, P. E., Mihashi, H., Huang, Y. Y., Zhang, X. H., & Nomura, N. (1987). Influence of age of loading, water-cement ratio and rate of loading on fracture energy of concrete. *Materials and structures*, *20*(2), 103-110.

Wittmann, F. H., Rokugo, K., Brühwiler, E., Mihashi, H., & Simonin, P. (1988). Fracture energy and strain softening of concrete as determined by means of compact tension specimens. *Materials and Structures*, *21*(1), 21-32.

Wittmann, F. H. (1992). Fracture process zone and fracture energy. *Fracture Mechanics of Concrete Structures. In: Proceeding of FraMCoS*, *1*, 391-403.

Zheng, W., Kwan, A. K. H., & Lee, P. K. K. (2001). Direct tension test of concrete. *Materials Journal*, *98*(1), 63-71.

Zu, G. Y., Lu, R. H., Li, X. B., Zhong, Z. Y., HAN, M. B., & YAO, G. C. (2013). Three-point bending behavior of aluminum foam sandwich with steel panel. *Transactions of Nonferrous Metals Society of China*, *23*(9), 2491-2495.

8. Appendices

Appendix 1: Cast trough bridges blueprint.

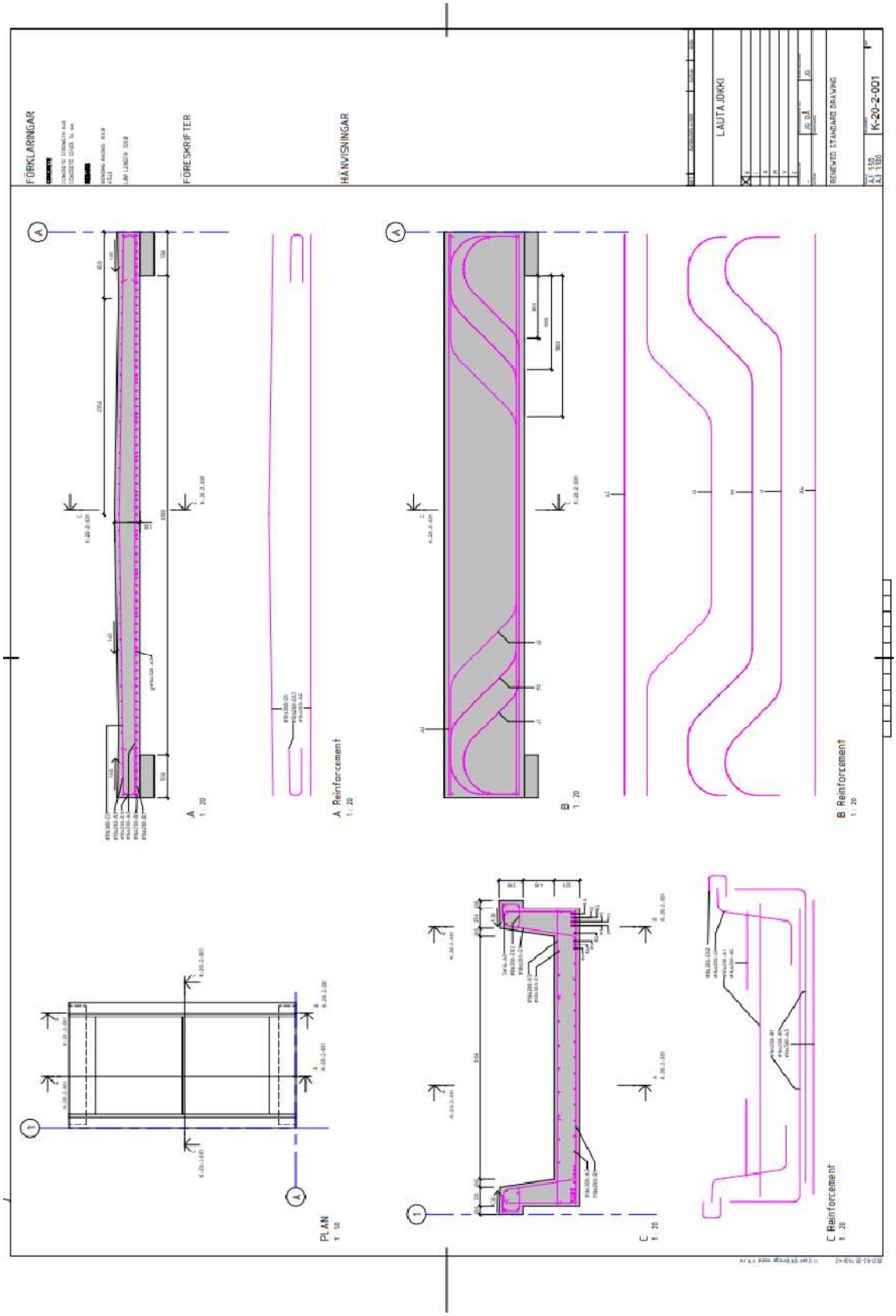

Appendix 2: Front view (a), top view (b) and isometric view (c) for the 100mm concrete core.

a) Front view

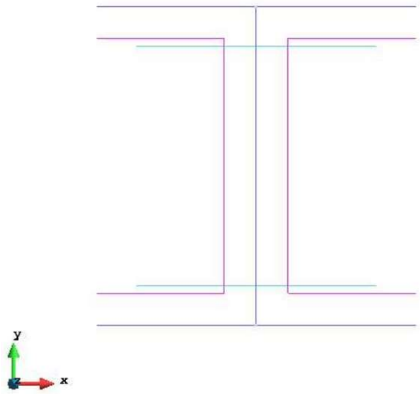

b) Top view

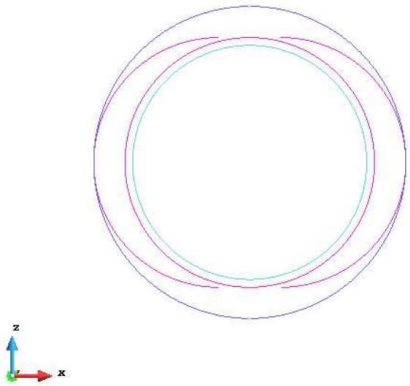

c) Isometric view

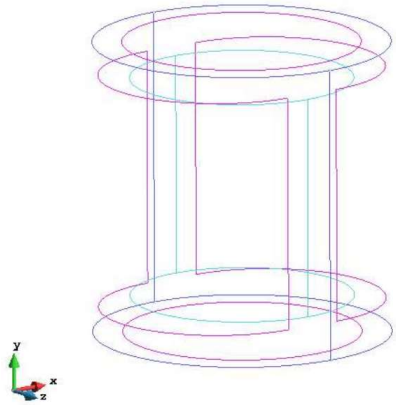

Appendix 3: Front view (a), top view (b), isometric view of the whole model (c), isometric view of the beam (d) and isometric view of a plate (e), for the concrete beam.

a) Front view

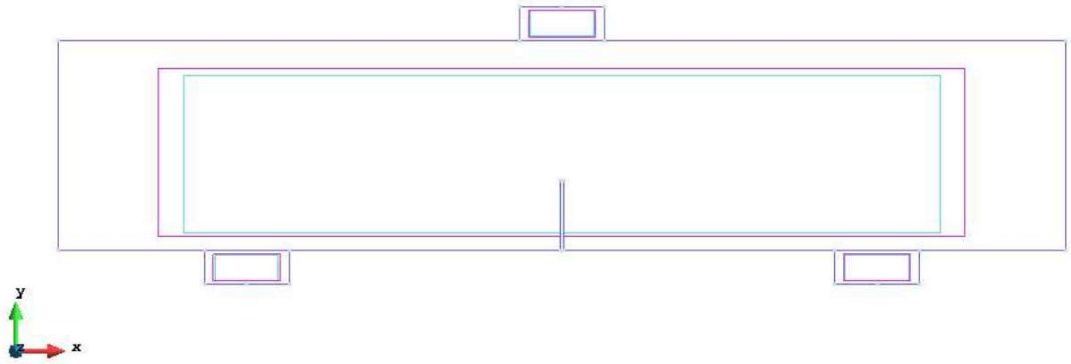

b) Top view

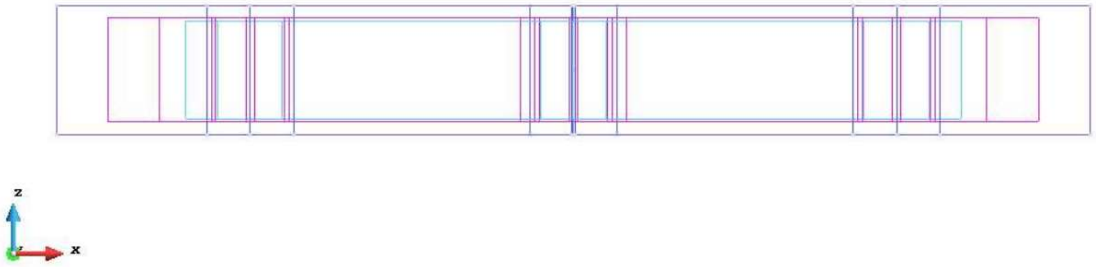

c) Isometric view of the whole model

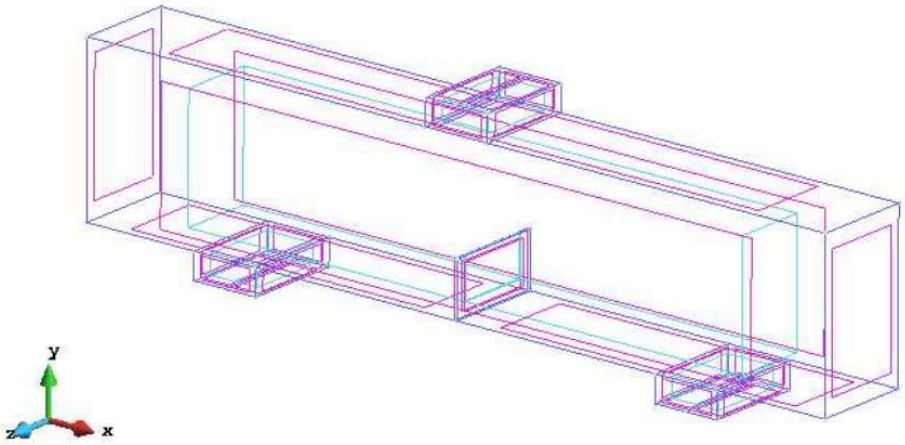

d) Isometric view of the beam

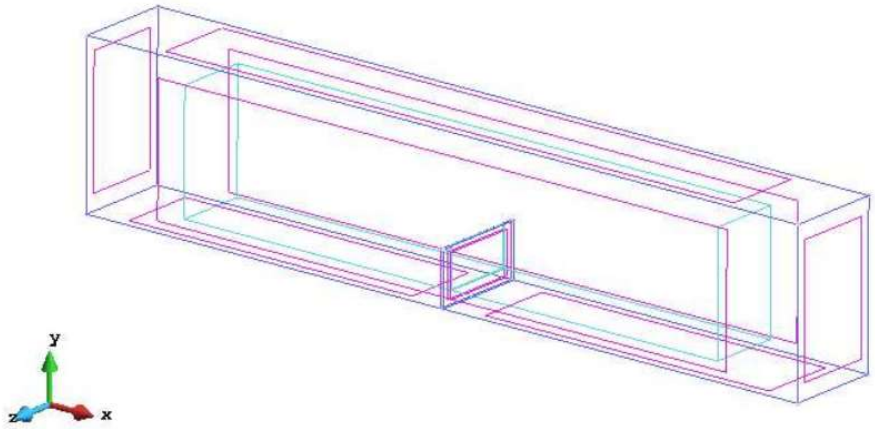

e) Isometric view of a plate

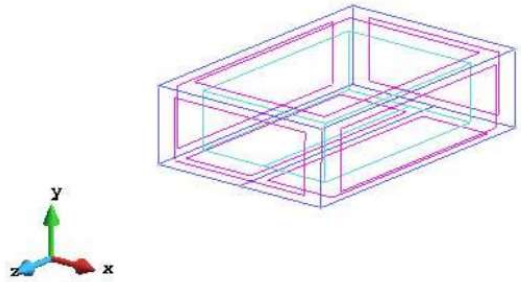

Appendix 4: Front view of the whole model (a), top view of the whole model (b), isometric view of the whole model (c), isometric view of the top/bottom cylinder (d) and isometric view of the middle cylinder (e) for the notched concrete core.

a) Front view of the whole model

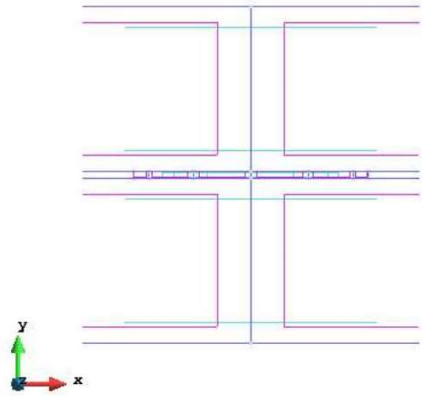

b) Top view of the whole model

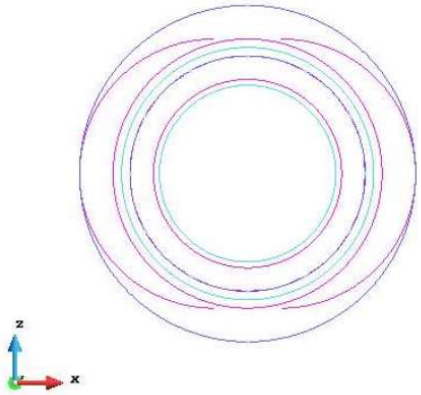

c) Isometric view of the whole model

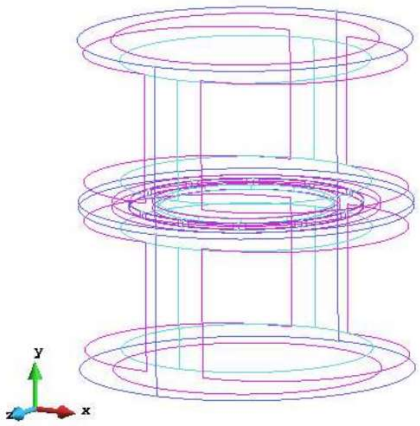

d) Isometric view of the top/bottom cylinder

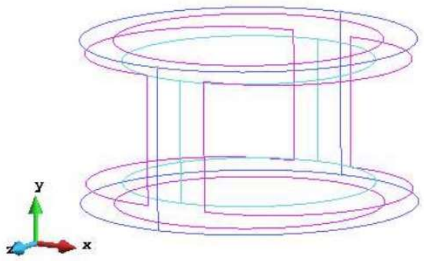

e) Isometric view of the middle cylinder